CHEMMEDCHEM

CHEMISTRY ENABLING DRUG DISCOVERY

Accepted Article

Title: Metal NHC Complexes with Naphthalimide Ligands as DNA-Interacting Antiproliferative Agents

Authors: Wojciech Streciwilk, Alessio Terenzi, Rainer Misgeld, Corazon Frias, Peter G. Jones, Aram Prokop, Bernhard Keppler, and Ingo Ott

To be cited as: *ChemMedChem* 10.1002/cmdc.201600557

Link to VoR: http://dx.doi.org/10.1002/cmdc.201600557

A Journal of

ChemPubSoc Europe

WILEY-VCH

www.chemmedchem.org

10.1002/cmdc.201600557

Metal NHC Complexes with Naphthalimide Ligands as DNA-Interacting Antiproliferative Agents

Wojciech Streciwilk,[a] Dr. Alessio Terenzi,[b,c] Rainer Misgeld,[d] Corazon Frias,[d] Prof. Dr. Peter G. Jones,[e] Dr. Aram Prokop,[d] Prof. Dr. Bernhard K. Keppler,[b,c] Prof. Dr. Ingo Ott [a]

[a] Institute of Medicinal and Pharmaceutical Chemistry, Technische Universität Braunschweig, Beethovenstr. 55, 38106 Braunschweig, Germany; [b] Institute of Inorganic Chemistry, University of Vienna, Waehringer Straße 42, A-1090 Vienna, Austria; [c] Research Platform "Translational Cancer Therapy Research", University of Vienna and Medical University of Vienna, Vienna, Austria; [d] Department of Paedriatric Oncology, Childrens Hospital Cologne, Amsterdamer Strasse 59, 50735 Cologne, Germany; [e] Institute of Inorganic and Analytical Chemistry, Technische Universität Braunschweig, Postfach 3329, 38023 Braunschweig, Germany.

Keywords:

anticancer, carbene, copper, naphthalimide, rhodium, ruthenium

10.1002/cmdc.201600557

TOC graphics

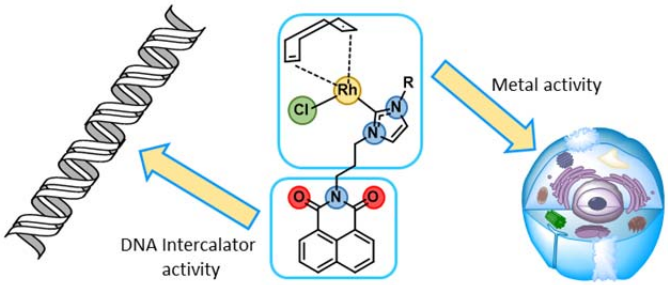

A stable rhodium(I) complex with a naphthalimide derived *N*-heterocyclic carbene ligand showed potent cytotoxic effects, interacted strongly with the DNA and induced apoptosis via mitochondrial pathways.

10.1002/cmdc.201600557

Abstract

Naphthalimide-based *N*-heterocyclic carbene (NHC) complexes of the type [(1,5-cyclooctadiene)(NHC)RhCl) (**4a-c**), [(*p*-cymene)(NHC)$RuCl_2$) (**5a-c**) and [(NHC)CuBr] (**6a-c**) were synthesised and investigated as antiproliferative agents that target DNA. The cytotoxic effects were largely driven by the naphthalimide structure, which represents a DNA intercalating moiety. Regarding the metal centre, the highest activities were observed with the rhodium complexes and the cytotoxic activity was strongly decreased for the ruthenium derivatives. The stable coordination of the NHC ligands of selected complexes **4b** and **5b** in solution was confirmed and their DNA-binding properties were studied by UV-vis and mass spectroscopies and also by circular dichroism. Stable intercalative binding into the DNA for all selected naphthalimide-based complexes is indicated by high DNA binding constants. Particularly efficient binding was noted in the case of the rhodium complex **4b**. More detailed biological studies on **4b** showed promising activities against multidrug-resistant Nalm-6 cells and confirmed an important role for mitochondrial pathways in **4b**-induced apoptosis.

10.1002/cmdc.201600557

Introduction

Following their great success in catalysis, metal complexes with *N*-heterocyclic carbene (NHC) ligands are nowadays increasingly used as building blocks for new metallodrugs in Inorganic Medicinal Chemistry.[1] The popularity of these organometallics is based on several advantages including the relatively high stability of their metal-carbon bonds and the convenient access to a large number of ligand structures by established synthesis procedures. Promising biological effects have been observed with various transition metals with a focus on gold and silver.

An interesting approach within this frame is the combination of metal NHC moieties with bioactive ligands or with structures containing a targeting functionality. Successful examples, which feature the combination of the biological properties of the respective ligand with those of a metal NHC fragment, include NHC derivatives of caffeine[2], peptides[3], combrestatin[4] or naphthalimides[5]. Among those, a gold(I) NHC naphthalimide derivative (see Figure 1) was confirmed to be a strong inhibitor of the enzyme thioredoxin reductase (related to the gold NHC fragment of the compound) and an effective DNA intercalator (related to the naphthalimide derived ligand structure).[5]

Naphthalimides are potent antiproliferative agents that intercalate into DNA strands as their major mode of drug action.[6] Selected examples (e. Amonafide) reached the clinical trial stages of drug development but eventually did not progress to therapeutic application. Nonetheless, the development of novel naphthalimide-based anticancer drug candidates is of high interest and an increasing number of reported active derivatives, including naphthalimide metal conjugates[5, 7] (see Figure 1), demonstrate their potential as future cancer chemotherapeutics.

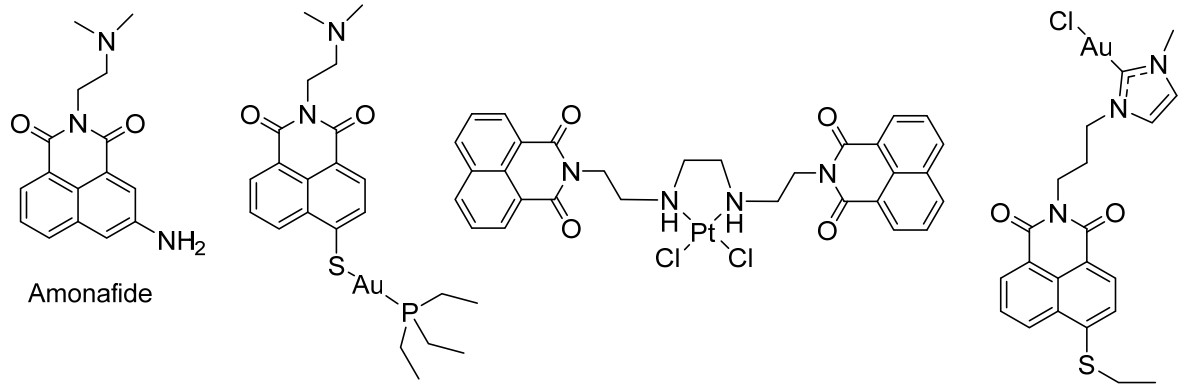

Figure 1: The anticancer naphthalimide Amonafide and examples of naphthalimide metal conjugates

In the paper we report on the extension of our efforts in the area of metal naphthalimide derivatives by introducing selected metal NHC fragments as bioactive partial structures into naphthalimide-derived ligands. Ruthenium(II), rhodium(I) and copper(I) metal centres were

chosen for this purpose, based on previous reports confirming their promising biological activities, which are related to various biochemical mechanisms: interaction with biological thiols and DNA (ruthenium NHC complexes)[8], binding to DNA and effects on cellular signalling (rhodium NHC complexes)[9], or interference with cellular redox mechanisms (copper NHC complexes).[10] The complexes were studied comparatively regarding their effects on cell proliferation, stability in solution and DNA interaction.

Results and discussion.

Synthesis

Naphthalimide-based *N*-heterocyclic carbene precursors **3a-c** were synthesized according to a slightly modified previous procedure.[5] Naphthalic anhydride (**1**) was heated with 1-(3'-aminopropyl)-imidazole at reflux in ethyl acetate to yield 3'-(-1'',8''-naphthalimid-N''-yl)-1-propyl-imidazole (**2**). The alkylation of the nitrogen of the imidazole in (**2**) was achieved by heating at reflux with an excess of an akyl halide in acetonitrile, leading to naphthalimide derivatives containing imidazolium halides in the side chain (**3a–c**). The target organometallic complexes were obtained by reacting **3a–c** with Ag_2O, leading to the formation of silver intermediates, and by a subsequent transmetallation reaction using: chlorido(1,5-cyclooctadiene)rhodium(I) (**4a-c**), dichloro(*p*-cymene)ruthenium(II) (**5a-c)** or bromo(dimethylsulphide)gold(I) (**6a-c**). The metal NHC complexes were isolated and purified by filtration over Celite. The final target complexes were recrystallized from dichloromethane/ethyl acetate (1:1) (**4a-c**), (3:1) (**5a-c**) and dried over P_2O_5.

In the ^{1}H NMR spectra of all three families of metal-NHC compounds, the absence of the imidazole C2 proton signal at δ = 9.1–9.3 ppm confirmed the formation of the organometallic carbon-metal bond. In some cases non equivalency of protons in the side chains was noted as previously reported.[8a] The identities of **4a–c**, **5a-c** and **6a–c** were further determined by mass spectrometry and their high purity was confirmed by elemental analysis, which differed by less than 0.5% from the theoretical values.

It is also noteworthy that, although the naphthalimide-based complexes have strong photophysical properties and many examples have been reported as efficient fluorescence sensors or imaging probes[6c, 11], the results obtained from fluorescence emission measurements of three selected complexes (**4b**, **5b**, **6b**) show that the metalation of the imidazole fragment quenches the emission of the naphthalimide chromophore (see Supporting Information).

10.1002/cmdc.201600557

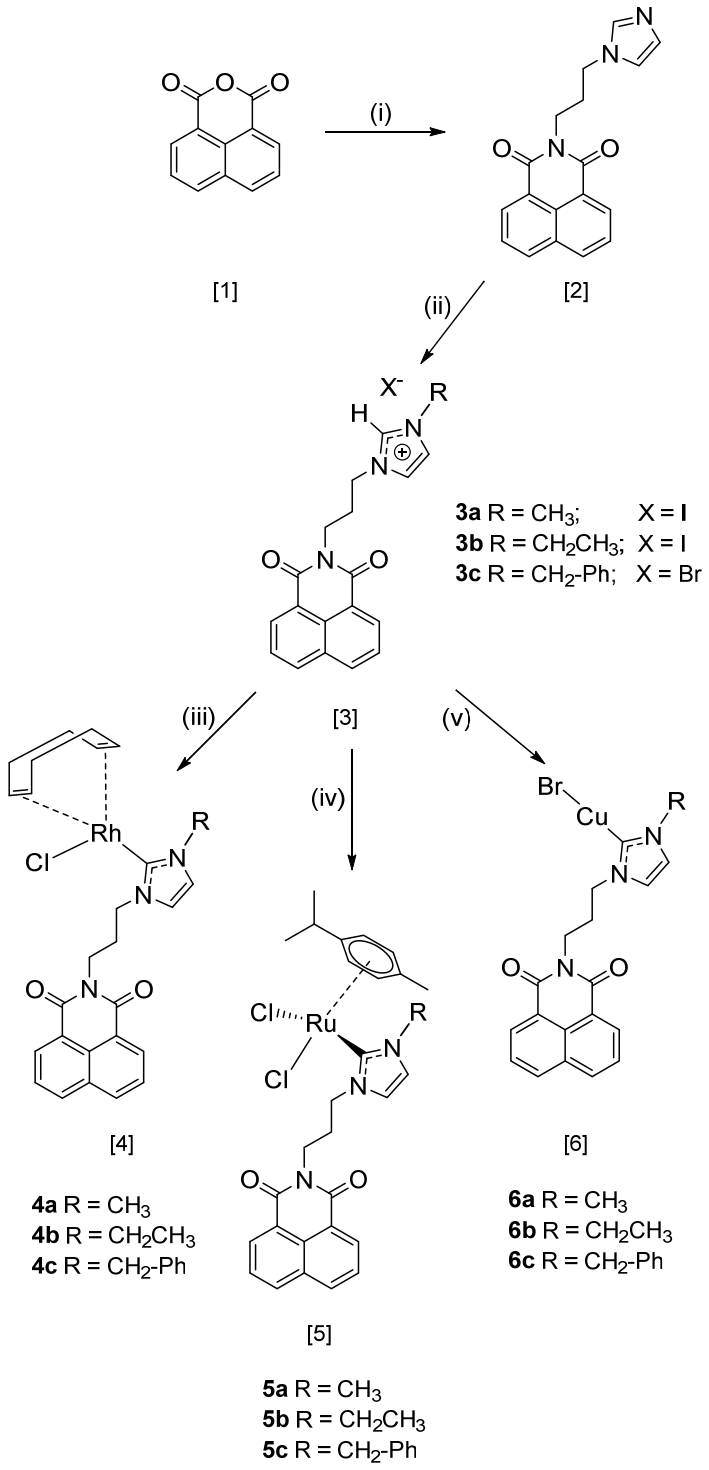

Scheme 1: Reagents and conditions: (i) 1.5 eq. 1-(3'-aminopropyl)-imidazole, ethyl acetate, reflux, 5 h; (ii) 3 eq. alkyl halide, acetonitrile, reflux, 2 h (**3a**), 6 h (**3b**), 12 h (**3c**); (iii) Step 1: 0.6 eq. Ag_2O, CH_2Cl_2, RT, stirred for 12 h; Step 2: 0.6 eq. $[Rh(COD)Cl]_2$, CH_2Cl_2, RT, 12-24 h; (iv) Step 1: 0.6 eq. Ag_2O, CH_2Cl_2, RT, stirred for 12 h; Step 2: 0.6 eq. $[Ru(p\text{-cymene})Cl_2]_2$, CH_2Cl_2, RT, 12-24 h; step 1: 0.6 eq. Ag_2O, CH_2Cl_2, RT, stirred for 12 h; step 2: 0.6 eq. CuBr-$S(Me)_2$, CH_2Cl_2, RT, 12-24 h.

10.1002/cmdc.201600557

The structure of compound **5b** was additionally evaluated by X-ray crystallography (see Fig. 2 and supporting information). The ruthenium atom lies 1.680 Å from the plane of the cymene ring, in which the bond lengths are somewhat increased (av. 1.425 Å) compared to the standard value for benzene; a survey of the Cambridge Database[12] data for ruthenium-cymene complexes showed that this may be regarded as usual (av. database value 1.411 Å). The carbene and naphthalimide ring systems subtend an interplanar angle of 80°

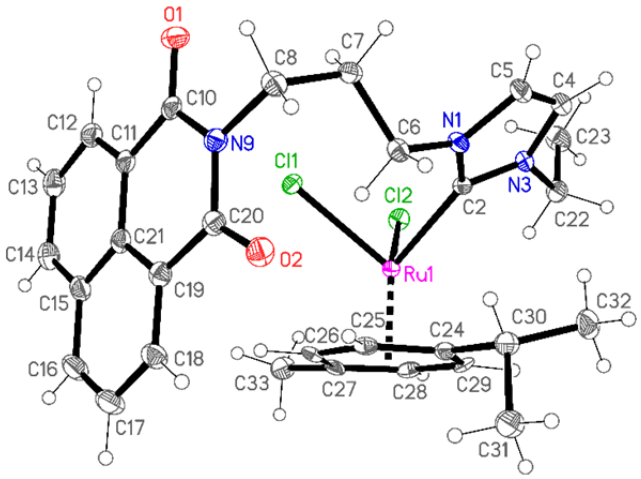

Fig. 2. The structure of compound **5b** in the crystal. Ellipsoids represent 50% probability levels. Selected bond lengths (Å): Ru1–Cl1 2.3931(5), Ru1–Cl2 2.4209(6), Ru1–C2 2.090(2).

Effects on tumor cell proliferation

The antiproliferative effects of **4-6** were evaluated in MCF-7 human breast adenocarcinoma and HT-29 colon carcinoma cells. Compounds **3a-c** were used as metal free references. Detailed inspection of the results summarised in Table 1 reveals several differences in the antiproliferative properties between the three families of investigated compounds. Naphthalimide rhodium derivatives **4a-c** triggered the strongest biological activity. The IC_{50} values of this series of compounds are below 10 μM in both cancer cell lines. Compared to the respective reference compounds **3a-c**, the magnitude of increase in their activity was 3- to 10-fold (with the exception of the similar activity of **4c** in MCF-7 cells). Moreover, the high cytotoxic activity was preserved throughout the series, irrespective of the substitution pattern of the imidazole fragment (R= methyl, ethyl or benzyl). In contrast to this, metalation of the naphthalimide-based ligand with the ruthenium *p*-cymene moiety, mostly resulted in the opposite effect. The ruthenium complex **5b** with an ethyl side chain on the imidazole lacks activity against both cancer cell lines, while its methyl congener **5a** shows moderate activity only against MCF-7 carcinoma cells. In contrast, complex **5c** with a benzyl group on the imidazole exhibits relatively high activity, comparable to its rhodium (**4c**) or copper (**6c**) analogues. The copper naphthalimide derivatives showed a specific structure-to-activity

relationship indicating the influence of lipophilicity on the antiproliferative potential. The least lipophilic complex **6a** is only moderately active against MCF-7 breast carcinoma and inactive against HT-29 colon carcinoma, while the most lipophilic derivative **6c** exhibits high activity against both cell lines. IC_{50} values of **6b** are almost exactly half-way between **6a** and **6c**. Notably, compound **6c** was the only copper complex that triggered higher activity compared with the corresponding metal-free reference (**3c**).

Overall, the results indicated that, for the complexes containing benzylimidazole ligands (**4c**, **5c**, **6c**), the cytotoxic effects are largely the consequence of the naphthalimide ligand (**3c**) with little contribution from the respective metal centres. This was not the case for the series of ethyl imidazole derivatives (**4b**, **5b**, **6b**). Here introduction of the rhodium fragment caused a clear increase of activity (compare results of **3b** with those of **4b**), while introduction of the ruthenium moiety led to inactivation (compare results of **3b** with **5b**) and the copper centre afforded a complex with similar activity (compare results of **3b** and **6b**).

Accordingly, complexes **4b** (active), **5b** (inactive) and **6b** (similar activity to the metal-free reference **3b**) appeared suitable for further comparative studies and were selected for the following experiments.

	3a	**3b**	**3c**	**4a**	**4b**	**4c**
MCF-7	9.2 ± 0.2	17.1 ± 1.7	5.2 ± 0.6	3.7 ± 0.1	3.7 ± 0.1	4.0 ± 0.2
HT-29	56.8 ± 0.7	31.3 ± 8.9	43.1 ± 10.2	5.1 ± 0.9	4.6 ± 0.3	9.8 ± 0.2
	5a	**5b**	**5c**	**6a**	**6b**	**6c**
MCF-7	55.4 ± 1.3	> 100	6.4 ± 0.6	27.4 ± 2.1	14.8 ± 0.8	2.0 ± 0.2
HT-29	> 100	> 100	14.2 ± 1.1	> 100	45.4 ± 3.6	3.1 ± 0.8

Table 1: IC_{50} values (μM) obtained in MCF-7 and HT-29 cells (presented as mean ± error of 3 repeated experiments); values for **3a-c** are taken from reference [5]

UV-vis spectroscopy

Initially the UV-vis spectra of compounds **3b**, **4b**, **5b**, **6b** were recorded in order to check for the presence of a linear relationship between absorbance and concentration according to the Lambert-Beer law and also to evaluate their stability in aqueous solutions (see Supporting Information). These are prerequisites for the DNA binding experiments described below, which are based on UV-vis spectroscopy. Although it was established in these experiments that all four compounds do indeed exhibit a linear relationship between absorption and concentration over the employed concentration range, the spectra indicated instability of the copper-based complex **6b** with partial decomposition in aqueous solution (see Supporting Information). Accordingly, compound **6b** was excluded from all following experiments.

10.1002/cmdc.201600557

Solution Stability of 4b and 5b

In order to study the solution stability of **4b** and **5b** further, the ^{1}H NMR spectra of the complexes of interest were measured in deuterated DMSO at 0 h, 6 h and 24 h.

The ^{1}H NMR spectrum of the (COD)(NHC)RhCl complex **4b** remained unchanged over the whole period of 24 h (see Supporting Information), which suggests that DMSO does not influence the stability of Rh-NHC and Rh-COD fragments of **4b**. For example, the single set of peaks for the COD ligand showed that the Rh-COD bonds do not undergo solvolysis and, therefore, the COD ligand remains coordinated. The ^{1}H NMR spectra, however, did not provide enough evidence to establish whether the complex loses the chlorido ligand. The lack of changes in spectra over time does not allow to distinction between a high stability of the Rh-Cl bond or its immediate dissociation with formation of solvent adducts upon dissolution of the compound.

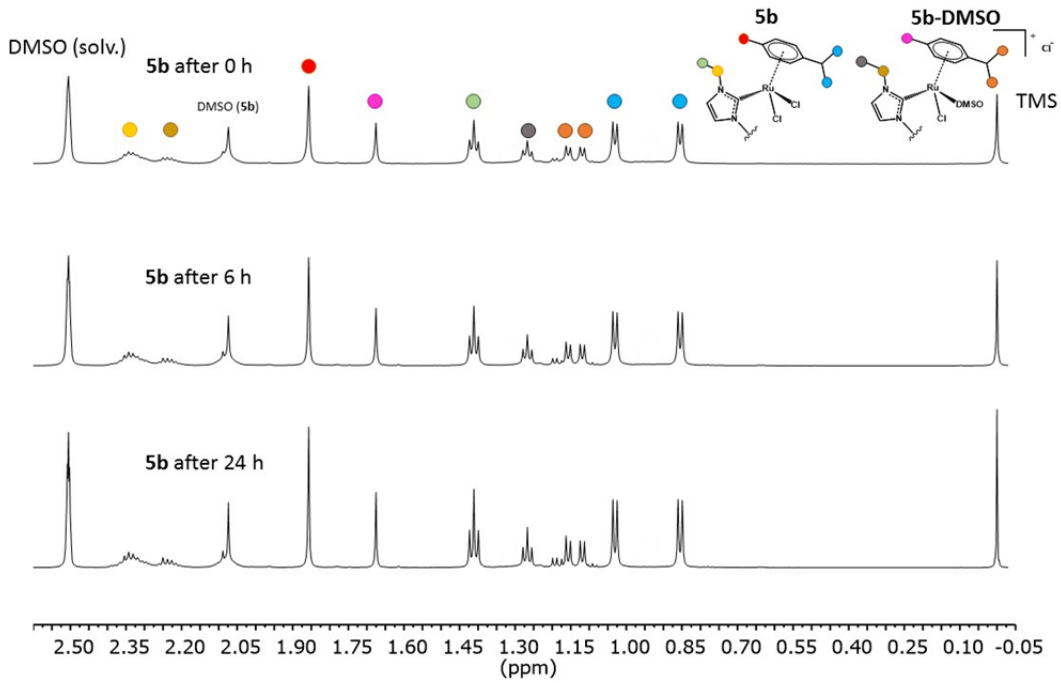

Figure 3. ^{1}H NMR spectra of ruthenium(II)-based complex **5b** in deuterated DMSO after 0 h (top), 6 h (middle) and 24 h (bottom). Chemical shifts are referenced to residual solvent peaks (DMSO: ^{1}H δ 2.50) and reported in parts per million (ppm). The signal at approx. 2.05 ppm could be assigned to **5b**-coordinated DMSO by comparison with literature values.[13] The full spectra are provided in the supporting information.

The time-dependent ^{1}H NMR spectra of **5b** were also identical, regardless of the time interval (Figure 3). However, duplicated peaks for the CH_3 groups of *p*-cymene and both methyl and ethyl groups of the 3-ethylimidazole, indicate the presence of two species in the DMSO-based ^{1}H NMR sample solution. Presumably, the two species represent the intact complex

10.1002/cmdc.201600557

5b and also a solvent adduct where one chlorido ligand has been replaced with DMSO. Since the signals were already observed at the beginning of the exposure period (time 0h), the chlorido/solvent exchange must have occurred and reached an equilibrium within a short time (a few minutes). To investigate the stability of **5b** further, the positive mode ESI-MS technique was applied. Samples for ESI-MS were diluted from 10 mM (DMSO) to 100 μM with water and measured at 0h, 1h and 24 h time intervals. These measurements further confirmed the release of one chlorido ligand (signal at m/z = 604.13, see Supporting Information).

DNA-binding: UV-vis spectroscopy

Binding to DNA can lead to changes in the UV-vis spectra of test compounds. Complexes **4b** and **5b** were exposed to increasing concentrations of DNA and their UV-vis spectra were recorded. The metal free imidazolium precursor **3b** was used as a reference. The aqueous buffer solutions (50 mM KCl, 5 mM Tris-HCl, pH = 7.5) of the compounds share an absorption band centred at 345 nm (black lines Figure 4 a, b and c) where DNA is transparent. Upon addition of calf thymus DNA (ct-DNA) solution aliquots, a large hypochromic effect for all recorded UV-vis spectra was observed. The decrease in absorbance was additionally accompanied by a small red-shift. These effects are similar to those reported for naphthalimide derivatives[7a, 14] and also for the well-known intercalator ethidium bromide.[15]

The data obtained from the above-mentioned measurements (absorbance vs DNA concentration) were fitted using the binding model proposed by Thordarson[16] to evaluate the binding constants (see Table 2). The intrinsic binding constant for the ruthenium complex **5b** was determined as 5.4 ± (0.4) x 10^3 M^{-1}, which is slightly higher than for the metal-free analogue **3b**. Interestingly, the binding constant for the rhodium analogue **4b** with ct-DNA was found to be 8.0 ± (0.9) x 10^4 M^{-1}, which is approximately one and a half orders of magnitude higher than the constants calculated for **3b** and **5b**. The binding constant of the fluorescent **3b** was further evaluated by fluorescence spectroscopy and this method afforded a similar result (see Supporting Information).

10.1002/cmdc.201600557

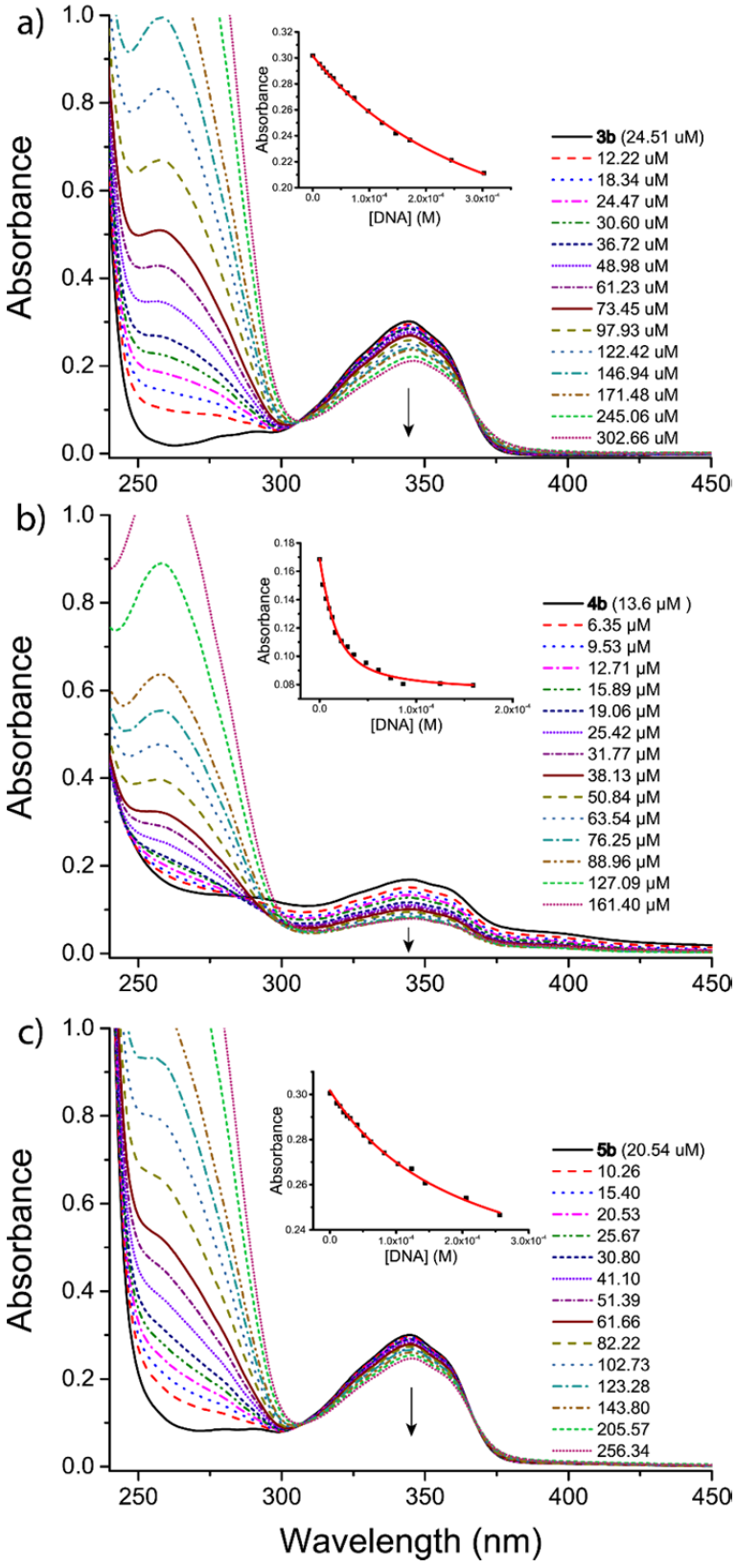

Figure 4. UV-vis titration of compounds a) **3b** (24.5 µM), b) **4b** (13.6 µM) and c) **5b** (20.5 µM) in the presence of increasing concentration of calf thymus DNA in. Arrows indicate the changes upon DNA addition. In the insets are represented the plots of Abs_{345nm} *vs* DNA concentration and the non-linear fits according to Equation 1 (red lines). Buffer: 50 mM KCl, 5 mM Tris-HCl, pH = 7.5.

	3b	4b	5b
K_b (M^{-1})	(3.1 ± 0.1) x 10^3	(8.0 ± 0.9) x 10^4	(5.4 ± 0.4) x 10^3

Table 2. DNA binding constants obtained from UV-vis DNA titrations.

DNA binding: Circular dichroism

Since the results of the UV-vis based DNA titrations confirmed that the complexes interacted with DNA, CD spectroscopy was used to further investigate their binding mode. For this purpose, changes in the typical CD spectrum of ct-DNA (positive band at 275 nm and negative band at 240 nm) were monitored during addition of increasing amounts of the metal complexes. The peak at 240 nm could not be evaluated, however, because of interference by the organic solvents (DMSO / DMF) in the stock solutions of **4b** and **5b**.

The CD spectra of DNA in the presence of increasing amounts of **3b**, **4b** and **5b**, up to a molar ratio R = [ML]/[DNA] = 2 are shown in Figure 5. The bands of native DNA are markedly modified by the addition of all three compounds indicating a relatively strong interaction of the naphthalimide derivatives within the DNA double helical structure.

In comparison to the metal-free reference compound **3b**, both the ruthenium and rhodium compounds **4b** and **5b** were able to induce CD (ICD) bands at around 350 nm when bound to the DNA structure. The most marked effect was caused by the rhodium-based compound **4b**, which interacted strongly with DNA confirming the results obtained by UV-vis experiments. Furthermore, plotting the CD signals in correspondence of the ICD band against the concentration of **4b**, and using Equation 1 (readapted for CD) for the non-linear fitting, a binding constant of 4.0 ± (0.5) x 10^4 could be calculated, which is of the same order of magnitude as the value obtained by UV-vis measurements. In detail, the equation used is the following:

$$Abs = \left\{ \varepsilon_f + \frac{\varepsilon_b K[DNA]_{tot}}{1 + 0.5\left\{-(1 - K[C]_{tot} + K[DNA]_{tot}) + \sqrt{(1 - K[C]_{tot} + K[DNA]_{tot})^2 + 4K[C]_{tot}}\right\}} \right\} \times \frac{-(1 - K[C]_{tot} + K[DNA]_{tot}) + \sqrt{(1 - K[C]_{tot} + K[DNA]_{tot})^2 + 4K[C]_{tot}}}{2K}$$

Equation 1, where ε_f (molar absorptivity of the naphthalimide-based derivative), $[DNA]_{tot}$ (total concentration of ct-DNA added) and C_{tot} (total concentration of the naphthalimide-based derivative) are known, while K (binding constant) and ε_b (molar absorptivity of the

10.1002/cmdc.201600557

naphthalimide-based derivative bound to ct-DNA) can be determined using the nonlinear regression analysis.

The combination of UV-vis and CD titrations thus indicates that the naphthalimide moiety is able to intercalate within the DNA as reported for other metal-naphthalimide derivatives[5, 7a, 14, 17] and that, remarkably, the coordinated rhodium metal centre enhances this effect.

10.1002/cmdc.201600557

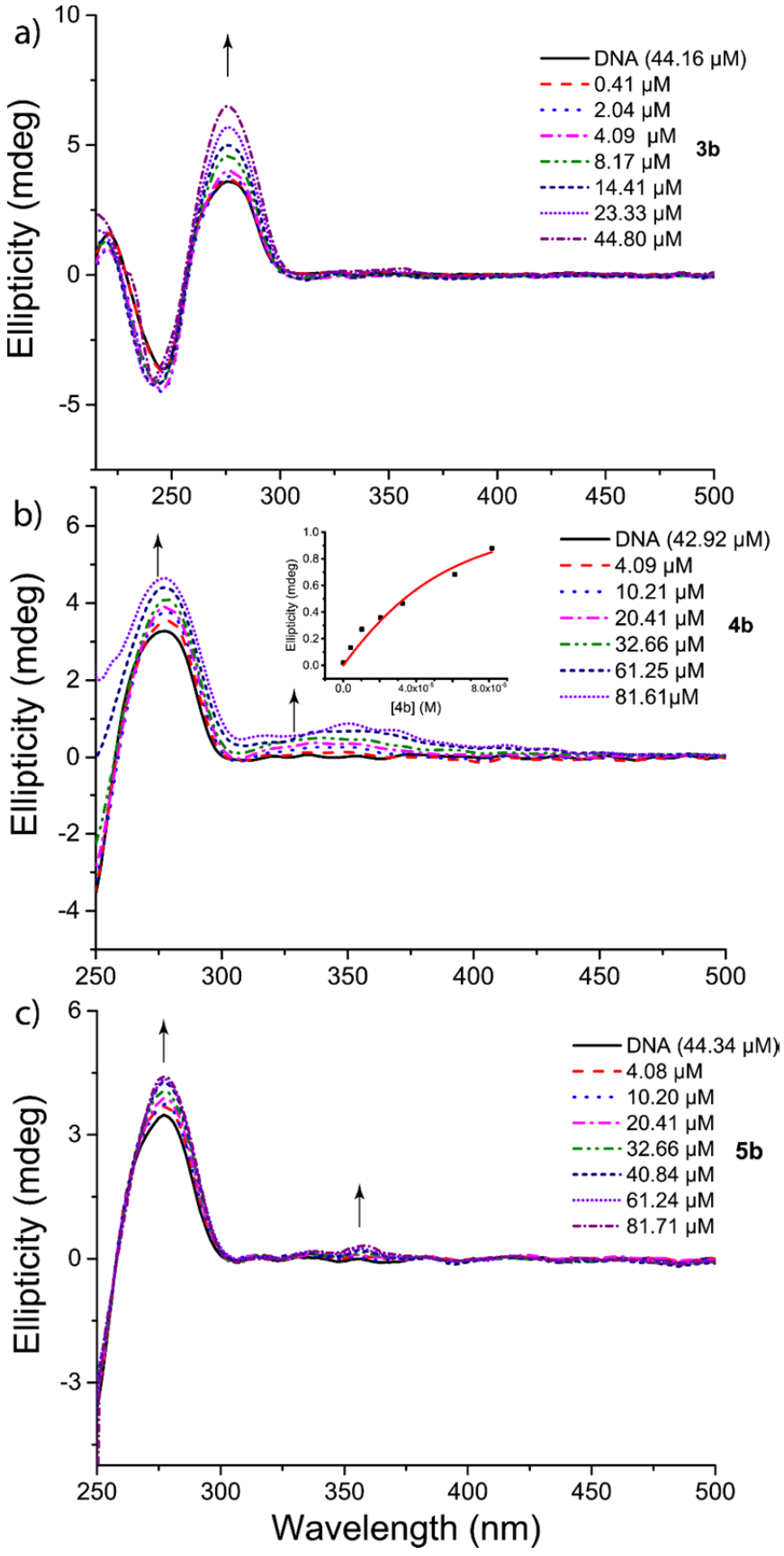

Figure 5. CD spectra of ct-DNA in the presence of increasing concentration of compounds a) **3b**, b) **4b** and c) **5b** (concentrations reported in the legend). Inset: plot of ellipticity at 350 nm *vs* 4b concentration and the non-linear fit according to Equation 1. Buffer: 50 mM KCl, 5 mM Tris-HCl, pH = 7.5.

10.1002/cmdc.201600557

DNA binding: reaction with 9-Ethylguanine

Ruthenium arene compounds are known to bind selectively to N7 of DNA base guanine.[18] To gain further insights into the binding mode of **4b** and **5b**, and in particular to assess whether they are able to bind DNA covalently besides intercalating via the naphthalimide moiety, a high resolution mass study of their interaction with the model nucleobase 9-ethylguanine (9-EtG) was performed. The complexes were exposed to 9-EtG in methanol/water mixtures over a period of 2 h and afterwards analysed by mass spectrometry. Importantly, the MS results (see Figures 6 and 7) showed that 9-EtG is able to coordinate to both rhodium and ruthenium in the metal NHC complexes **4b** and **5b**, with loss of a chlorido ligand.

Taken together, compound **4b** combines an efficient cytotoxic effect with a profound DNA interaction and thus represents the most promising compound of all of those here investigated. Accordingly, further studies on the anticancer mechanisms were focused on **4b**.

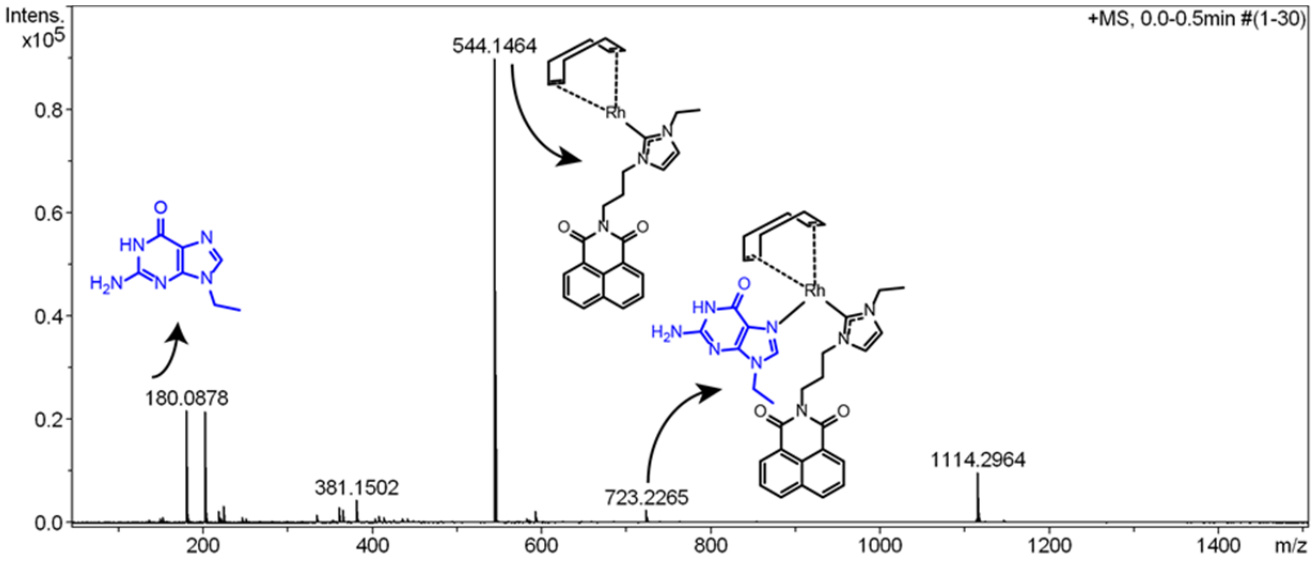

Fig. 6: Mass spectrum of the 9-ethylguanine incubated with the rhodium complex **4b**. Final concentrations in MeOH / H_2O before injection were 0.2 mM for **4b** and 0.6 mM for 9-EtG.

10.1002/cmdc.201600557

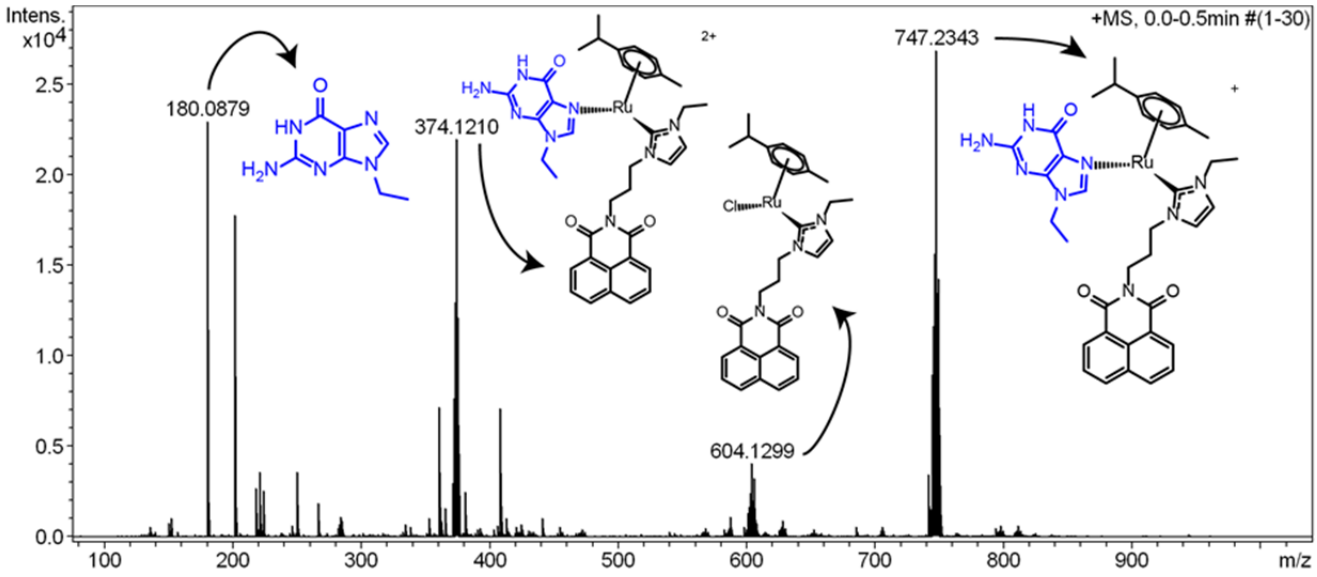

Fig. 7: Mass spectrum of the 9-ethylguanine incubated with the ruthenium complex **5b**. Final concentrations in MeOH / H_2O before injection were 0.2 mM for **5b** and 0.6 mM for 9-EtG.

Apoptosis induction in resistant cells by 4b

Drug resistance represents a major problem in current cancer chemotherapy. To examine the ability of **4b** to overcome drug resistance we investigated its apoptosis-inducing effects in the leukemia cell line Nalm-6 and also in its multidrug-resistant p-glycoprotein overexpressing vincristine- (Nalm-6/VCR) and daunorubicine-resistant (Nalm-6/DNR) sublines.[19] Initially, suitable effective concentration ranges were determined in preliminary experiments (LDH release, proliferation, see Supporting Information).

The ability of **4b** to induce apoptosis was evaluated by determination of the number of cells with fragmented DNA after 72 h of incubation with **4b**. In both multidrug resistant cell lines **4b** effectively induced apoptosis in concentrations above 1.0 µM (see Figure 8 and Supporting Information). In good agreement with previous reports on other rhodium NHC complexes[9c] this indicates that **4b** is not a substrate for the p-glycoprotein drug efflux pump.

10.1002/cmdc.201600557

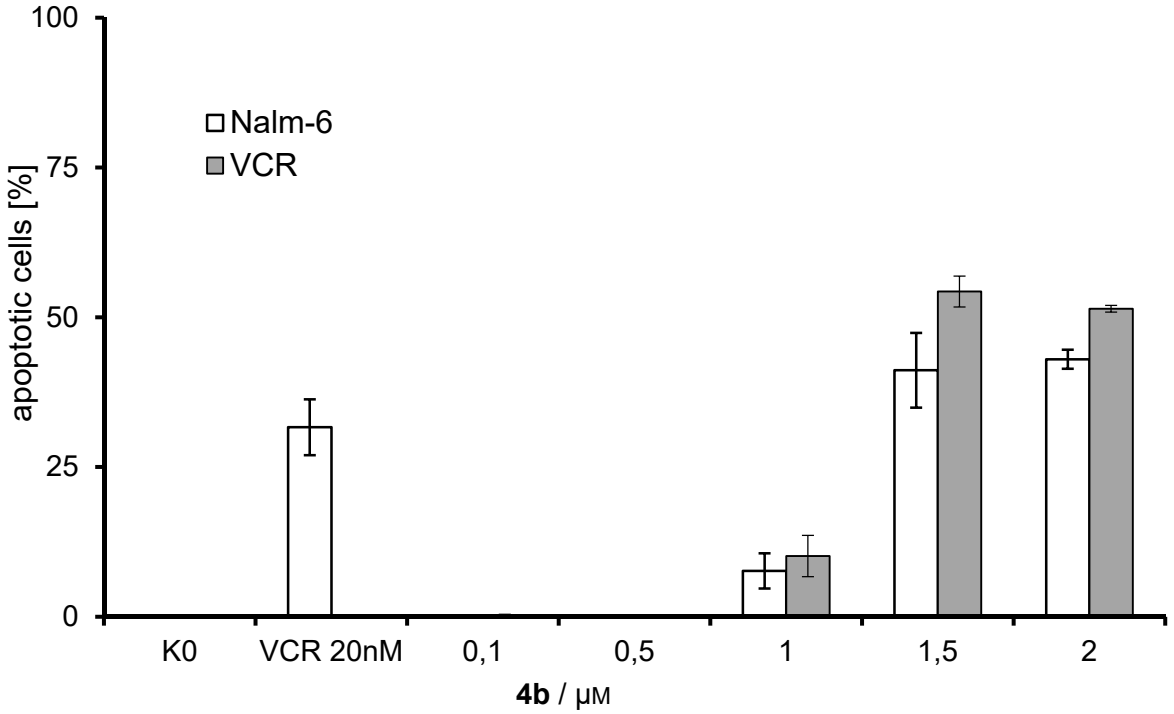

Figure 8: Apoptosis induction by **4b** determined as nuclear DNA fragmentation after 72 h drug exposure in wild-type Nalm- 6 cells and also in vincristine-resistant (VCR) subtypes. Data are given as percentages of cells with hypodiploid DNA ±SD (n=3). Resistance to vincristine was confirmed by the absent or very low apoptosis induction after exposure to VCR 20 nM. Similar results were obtained with daunorubicine resistant Nalm-6 cells (see Supporting Information).

Effects of 4b on important apoptosis pathways

In order to characterize **4b**-induced apoptosis in more detail, effects on Bcl-2 and mitochondrial membrane potential were studied. Bcl-2 is known to be an anti-apoptotic member in the mitochondrial pathway. Up-regulation of Bcl-2 has been reported leading to resistance against many cytostatic drugs in human melanoma cells (MelHo). To determine Bcl-2 independency we used the cell system MelHo pIres/Bcl-2, whereby the Bcl-2 line strongly overexpresses the anti-apoptotic Bcl-2 protein through stable transfection with the pIres-Bcl-2 vector. The MelHO Bcl-2 cell line underwent apoptosis at a lower level than the control cell line treated with **4b**; however, apoptosis was not completely blocked (Figure 9).

The loss of the mitochondrial membrane potential is followed by release of cytochrome-c in the early phase of the intrinsic apoptotic pathway, which leads to caspace-9-activation. To examine the involvement in this pathway, Nalm-6 cells were examined by flow cytometric analysis after incubation for 48 h with various concentrations of **4b**. Figure 10 shows an increase of cells with low mitochondrial membrane potential from 14% with 1.0 µM **4b** to nearly 50 % with 2.0 µM. These findings indicate that the mitochondrial pathway plays an important role in **4b**-induced apoptosis.

10.1002/cmdc.201600557

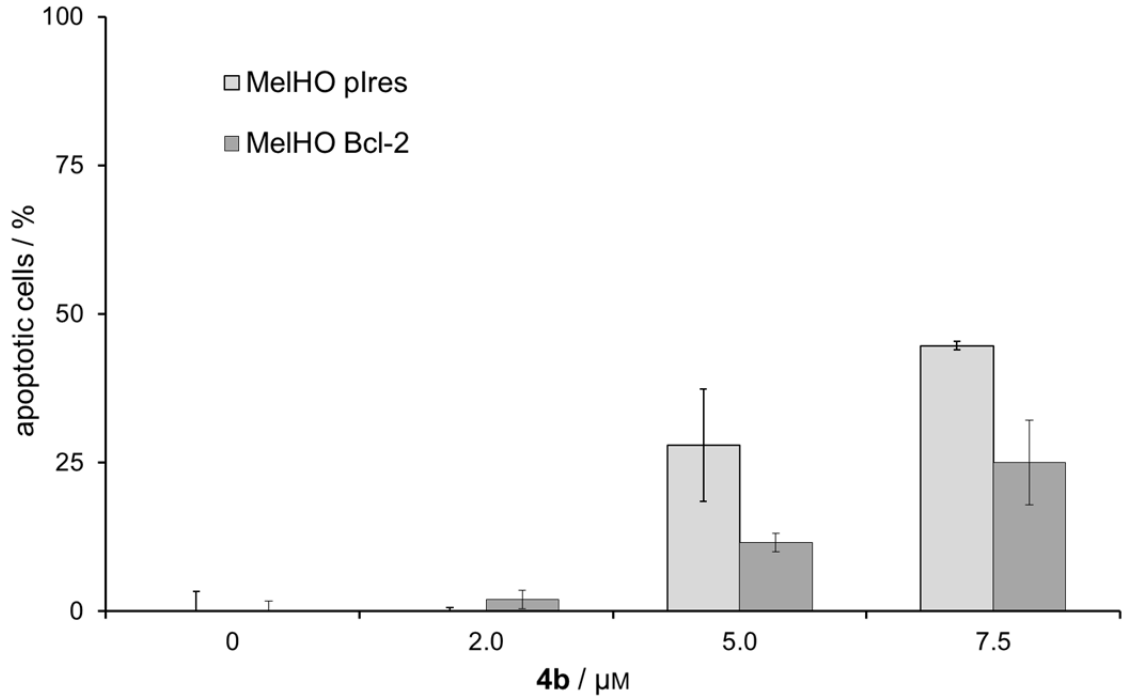

Figure 9: MelHO Bcl-2 cells (overexpressing anti-apoptotic Bcl-2 protein) and MelHO pIres cells were either incubated with **4b** at different concentrations or left untreated as control. After 72 h, DNA fragmentation was measured by flow cytometric analysis. Data are given as percentages of cells with hypodiploid DNA ±SD (n=3).

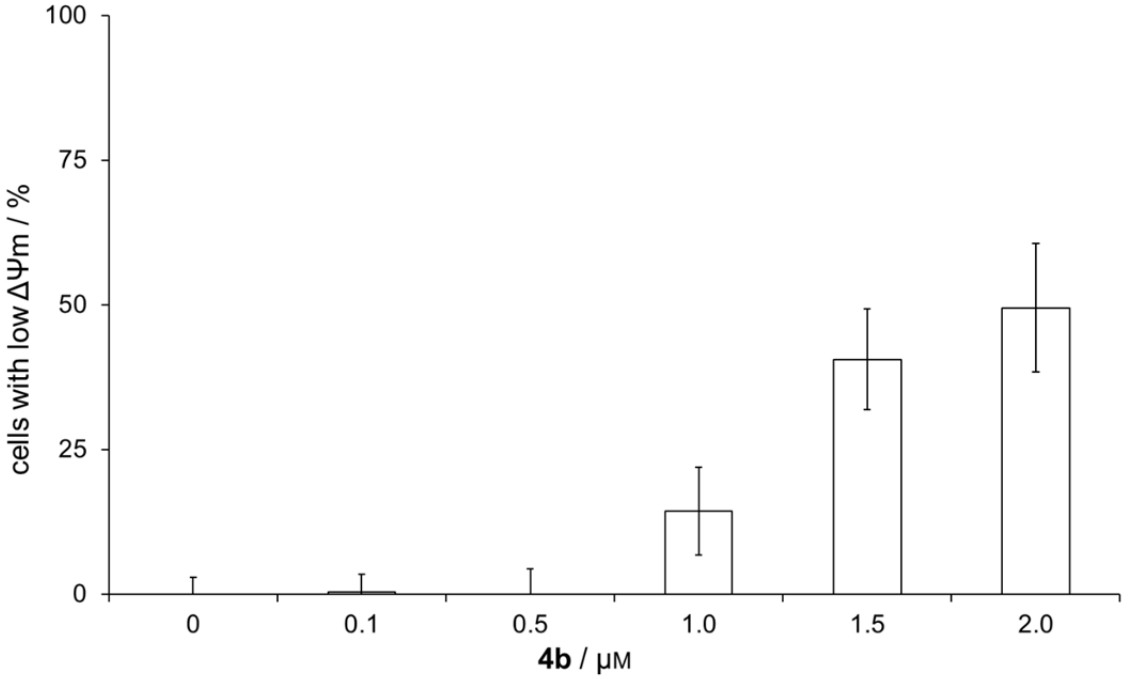

Figure 10: Influence of **4b** on the mitochondrial membrane potential. The mitochondrial permeability transition was measured by flow cytometric analysis after 48 h of incubation of Nalm-6 cells with **4b**. Results of the mitochondrial permeability transition are given as the fraction of cells with decreased membrane potential (ΔΨm) in%±SD (n=3).

Conclusions

Organometallic naphthalimide-derivatives with a ruthenium(II), rhodium(I) or copper(I) NHC substructure can be conveniently prepared starting from naphthalic anhydride. Evaluation of the antiproliferative effects in cancer cells showed in particular that the introduction of the rhodium NHC fragment caused enhanced cytotoxic activity, whereas the ruthenium NHC complexes triggered low activity or were inactive. For copper NHC complexes lipophilicity appears to play an important role for obtaining antiproliferatively active complexes. Inactivity of some ruthenium NHC complexes in cytotoxicity experiments had been observed in previous studies and was probably the consequence of a low bioavailability.[2c, 8]

Based on the cancer cell proliferation data compounds **3b**, **4b**, **5b** and **6b** were selected for further screening of their DNA-interacting properties. Preliminary evaluation of their UV absorption properties, however, indicated insufficient stability of the copper-based complex **6b** and the compound was therefore excluded from further experiments.

The stability of complexes **4b** and **5b** was followed in DMSO by NMR spectroscopy and additionally in a water / DMSO mixture by MS spectroscopy in the case of **5b**. Taken together, these experiments confirmed a high stability of the NHC and also of the COD and p-cymene ligands. The stability of the chlorido ligand of the rhodium derivative **4b** was not established; however, there was strong evidence for the replacement of one chlorido ligand of the ruthenium complex **5b** upon interaction with solvents.

Regarding rhodium(I) NHC complexes, previous studies on a derivative that contained an electron-withdrawing (probably destabilized) NHC ligand, had also shown a high stability of the coordinated ligands over several hours. However, after longer exposure hydrolysis of the chlorido ligand was observed, accompanied by a loss of the NHC ligand and dimerization.[9b] Since there was no evidence for a loss of the NHC and COD ligands of **4b**, its NHC ligand might provide a sufficiently stable rhodium-carbon bond to perform extended biological studies.

The hydrolysis of chlorido ligands of ruthenium arene complexes is well established in Inorganic Medicinal Chemistry and the observations concerning solvolysis of the chlorido ligands of **5b** are consistent with this.[20] It should be noted here that we had observed a mobilisation of the NHC and arene ligands of Ru(II) NHC complexes upon interaction with thiols in a previous study.[8a]

The differences in cytotoxicities between **4b** and **5b** might be the consequence of different reactivity in biological media. On the one hand a good biological stability can be expected for **4b** and as a neutral compound it should enter cells efficiently. On the other hand **5b** is likely to easily exchange a chlorido ligand with extracellular proteins (similar to other ruthenium metallodrugs[21]) and this would hamper its bioavailability.

With the help of UV-vis based ct-DNA titration, it was established that **4b** and **5b** and also the metal-free naphthalimide reference compound **3b** interacted with DNA, and comparison of the binding constants showed positive effects especially in the case of the rhodium derivative **4b**. Moreover, CD measurements indicated the stabilisation of the DNA strands via intercalation of the naphthalimide subunit. Notably, the rhodium complex **4b** produced the most pronounced effects on the DNA CD spectrum, with the appearance of a clear ICD band.

Mass spectrometry experiments showed that the chlorido ligands of **4b** and **5b** can be replaced by 9-EtG suggesting a possible role of coordinative binding to nucleobases.

Taken together, it can therefore be speculated that the complexes show a dual mode of DNA binding, which is based on (naphthalimide related) intercalation and (metal-related) coordinative binding to nucleobases.

Complex **4b** represented a compound with very high cytotoxic effects in combination with a particularly strong binding to the DNA. Therefore, further studies regarding the apoptosis inducing properties focused on this compound. Interestingly, **4b** effectively induced apoptosis in both resistant (p-glycoprotein overexpressing) and wildtype Nalm-6 cells and this indicates that the compound might be used for the treatment of multidrug resistant cancers. Apoptosis was partially reversed by the anti-apoptotic protein Bcl-2, and mitochondrial pathways are probably key players in **4b**-induced apoptosis.

In conclusion, the results show that the newly synthesised series of complexes show promising biological properties towards the application as new anticancer agents. Further application and evaluation of these series of complexes is the subject of ongoing research.

Experimental

General

All solvents and reagents were purchased from commercial suppliers (Sigma-Aldrich, Fisher, Fluka) and were of analytical grade. Dichloromethane was further dried over calcium hydride and collected by distillation. ^{1}H NMR spectra were recorded on a Bruker DRX-400 AS NMR spectrometer and ^{13}C NMR spectra on a Bruker AV II-600 AS NMR spectrometer. Chemical shifts are reported in parts per million and referenced to residual solvent peaks ($CDCl_3$: ^{1}H δ 7.26, ^{13}C δ 77.16). Coupling constants (*J*) are reported in Hertz (Hz). MS spectra (ESI) were recorded on a ThermoFisher Scientific LTQ-Orbitrap Velos operated in positive-ion mode. The purity of the target compounds was confirmed by elemental analysis (Flash EA1112, Thermo Quest Italia). Melting points were determined using a FisherScientific™ Digital Melting Point Apparatus and are uncorrected.

Lyophilized calf thymus DNA (Fluka, BioChemika) was resuspended in 1.0 mM tris-hydroxymethyl-aminomethane (Tris-HCl) pH = 7.5. DNA concentration, expressed in monomers units, was determined by UV spectrophotometry using 6600 M^{-1} cm^{-1} as molar absorption coefficient at 260 nm. All DNA intercalation experiments were carried in 50 mM KCl, 5 mM Tris-HCl aqueous buffer at pH = 7.5. Previously reported methods were used to prepare **2** and (**3a–c**).[5]

Synthesis

General procedure for synthesis of the metal NHC complexes 4a–c, **5a–c** and **6a–c**: The appropriate imidazolium halide **3a–c** (0.25 mmol, 1 eq.) and Ag_2O (0.6 eq.) were transferred to a dry Schlenk tube. The mixture was treated with N_2 (3x), and then CH_2Cl_2 (10 mL) was added. For the synthesis of **6a–c** predried (over CaH) and freshly distilled dichloromethane was used. The flask was closed, and the mixture was stirred for 24h at RT in the dark. A solution of chloro(1,5-cyclooctadiene) rhodium(I) dimer (**4a–c**), dichloro(*p*-cymene)ruthenium(II) dimer (**5a–c**), or copper(I) bromide dimethylsulfide (**6a–c**) in CH_2Cl_2 (0.125 mmol, 0,5 eq., in 10 mL) were added and the reaction mixture was stirred for another 12–24 h at RT in the dark. The suspension thus obtained was filtered over Celite (281 nm), and the solvent was removed at 900 mbar and 40°C to prevent decomposition. The solid product was recrystallized from Et_2O and dried over P_2O_5.

Chlorido[(η^2,η^2-cycloocta-1,5-diene)-1-(3'-(1'',8''-naphthalimid-N''-yl))-propyl-3-methyl-imidazol-2-ylidene]rhodium(I) (**4a**)

Yield: 0.032 g (0.05 mmol, 23%) yellow crystals; melting point: 216–225 °C (thermal decomposition); ^{1}H NMR ($CDCl_3$): (ppm) δ 8.64 (dd, ^3J = 7.3 Hz, ^4J = 1.2 Hz, 2H, Ar$H_{4/5}$), 8.24 (dd, ^3J = 8.3 Hz, ^4J = 1.1 Hz, 2H, Ar$H_{2/7}$), 7.77 (dd, ^3J = 8.3 Hz, ^3J = 7.3 Hz, 2H, Ar$H_{3/6}$), 7.04 (d, ^3J = 2.0 Hz, 1H$_{imidazolylidene}$), 6.83 (d, ^3J = 1.9 Hz, 1H$_{imidazolylidene}$), 4.94 (td, ^3J = 7.9 Hz 1H, C*H*-COD), 4.83 (td, ^3J = 8.0 Hz, 1H, C*H*-COD) 4.68 (dt, ^3J = 8.6 Hz, 2H, NCH_2CH$_2$-), 4.36 (dt, ^3J = 7.5 Hz, 2H, -CH$_2$CH_2N), 4.06 (s, 3H, NCH_3), 3.31 (m, 1H, C*H*-COD), 3.25 (m, 1H, C*H*-COD) 2.56 – 2.14 (m, 6H, CH_2-COD), 1.88 (m, 4H, CH_2-COD, NCH$_2$CH_2-); ^{13}C NMR ($CDCl_3$): (ppm) δ 182.32 (ArC2), 164.25 (CO), 134.08 (ArC), 131.59 (ArC), 131.36 (ArC), 128.19 (ArC), 126.98 (ArC), 122.57 (ArC), 122.08 (CH$_{imidazolylidene}$), 120.22 (CH$_{imidazolylidene}$), 98.52 (d, ^1J = 6.8 Hz, CH-COD), 98.29 (d, ^1J = 6.8 Hz, CH-COD), 68.02 (d, ^1J = 14.6 Hz, CH-COD), 67.70 (d, ^1J = 14.6 Hz, CH-COD), 48.51 (NCH$_2$-), 37.98 (NCH$_2$-), 37.74 (NCH$_3$), 33.07 (CH$_2$-COD), 32.74 (CH$_2$-COD), 29.44 (NCH$_2$CH$_2$CH$_2$N), 28.88 (CH$_2$-COD), 28.69 (CH$_2$-COD); MS(ESI): 530.13 (M + Cl^-); elemental analysis for $C_{27}H_{29}N_3O_2ClRh$ (% calcd./found): C (57.31/57.34), H (5.17/5.05), N (7.43/7.07).

Chlorido[(η^2,η^2-cycloocta-1,5-diene)-1-(3'-(1'',8''-naphthalimid-N''-yl))-propyl-3-ethyl-imidazol-2-ylidene]rhodium(I) (**4b**).

Yield: 0.076 g (0.13 mmol, 53%) yellow crystals; melting point: 214–223 °C (thermal decomposition); ^{1}H NMR ($CDCl_3$): (ppm) δ 8.63 (dd, ^3J = 7.3 Hz, ^4J = 1.2 Hz, 2H, Ar$H_{4/5}$), 8.22 (dd, ^3J = 8.3 Hz, ^4J = 1.2 Hz, 2H, Ar$H_{2/7}$), 7.77 (dd, ^3J = 8.2 Hz, ^3J = 7.3 Hz, 2H, Ar$H_{3/6}$), 7.06 (d, ^3J = 1.9 Hz, 1H$_{imidazolylidene}$), 6.87 (d, ^3J = 2.0 Hz, 1H$_{imidazolylidene}$), 4.92 (td, ^3J = 5.4 Hz, 1H, C*H*-COD), 4.84 (td, ^3J = 7.7 Hz, 1H, C*H*-COD), 4.68 (dt, ^3J = 8.6 Hz, 2H, NCH_2CH$_3$-), 4.64 (q, ^3J = 7.2 Hz, 1H, NCH_2CH$_3$), 4.49 (q, ^3J = 7.3 Hz, 1H, NCH_2CH$_3$), 4.37 (dt, ^3J = 7.5 Hz, 2H, -CH$_2$CH_2N), 3.33 – 3.23 (m, 2H, C*H*-COD), 2.56 – 2.15 (m, 6H, CH_2-COD), 1.87 (m, 4H, CH_2-COD, NCH$_2$CH_2-), 1.51 (t, ^3J = 7.3 Hz, 3H, NCH$_2$CH_3); (600 MHz, DMSO-d_6): (ppm) δ 8.55 (dd, ^3J = 7.3 Hz, ^4J = 1.2 Hz, 2H, Ar$H_{4/5}$), 8.48 (dd, ^3J = 8.4 Hz, ^4J = 1.1 Hz, 2H, Ar$H_{2/7}$), 7.90 (dd, ^3J = 8.2 Hz, ^3J = 7.2 Hz, 2H, Ar$H_{3/6}$), 7.33 (d, ^3J = 2.0 Hz, 1H$_{imidazolylidene}$), 7.28 (d, ^3J = 1.9 Hz, 1H$_{imidazolylidene}$), 4.61 (t, ^3J = 5.4 Hz, 1H, C*H*-COD), 4.54 (t, ^3J = 7.7 Hz, 1H, C*H*-COD), 4.47 – 4.37 (m, 2H, NCH_2CH$_2$-), 4.32 (q,^3J = 7.2 Hz, 2H, NCH_2CH$_3$), 4.28 – 4.19 (m, 2H, -CH$_2$CH_2N), 4.15 (td, ^3J = 7.9 Hz, 2H, NCH_2CH$_3$), 3.16 (t, ^3J = 7.4 Hz, 1H, C*H*-COD), 3.09 (t, ^3J = 7.7 Hz, 1H, C*H*-COD) 2.43 – 2.33 (m, 2H, CH_2-COD), 2.28 – 2.03 (m, 4H, CH_2-COD), 1.77 – 1.63 (m, 2H, NCH$_2$CH_2-), 1.63 – 1.55 (t, 2H, CH_2-COD), 1.49 (t, 2H, CH_2-COD), 1.37 (t, ^3J = 7.3 Hz, 3H, NCH$_2$CH_3); ^{13}C NMR ($CDCl_3$): (ppm) δ 181.77 (NHC), 164.23 (CO), 134.05 (ArC), 131.59 (ArC), 131.34 (ArC), 128.20 (ArC), 126.97 (ArC), 122.60 (ArC), 120.38 (CH$_{imidazolylidene}$), 119.71 (CH$_{imidazolylidene}$), 98.46 (d, ^1J = 7.0 Hz, C*H*-COD), 98.00 (d, ^1J = 6.9 Hz, CH-COD), 67.89 (dd, ^3J = 14.6, , ^3J = 10.7 Hz, 2C, CH-COD), 48.59 (NCH$_2$-), 45.61 (N<u>C</u>H$_2$CH$_3$), 38.01 (NCH$_2$-), 33.02 (CH$_2$-COD), 32.78 (CH$_2$−COD), 29.42 (NCH$_2$<u>C</u>H$_2$CH$_2$N), 28.88 (CH$_2$-COD), 28.68 (CH$_2$-COD), 16.27 (NCH$_2$<u>C</u>H$_3$); MS(ESI): 544.14 (M + Cl^-); elemental analysis for $C_{28}H_{31}N_3O_2ClRh$ (% calcd/found): C (57.99/58.13), H (5.39/5.31), N (7.25/7.04).

Chlorido[(η^2,η^2-cycloocta-1,5-diene)-1-(3'-(1'',8''-naphthalimid-N''-yl))-propyl-3-benzyl-imidazol-2-ylidene]rhodium(I) (**4c**).

Yield: 0.122 g (0.19 mmol, 76%) yellow soli; melting point: 218–228 °C (thermal decomposition); ^{1}H NMR ($CDCl_3$): (ppm) δ 8.64 (dd, ^3J = 7.3 Hz, ^4J = 1.2 Hz, 2H, Ar$H_{4/5}$), 8.24 (dd, ^3J = 8.4 Hz, ^4J = 1.1 Hz, 2H, Ar$H_{2/7}$), 7.77 (dd, ^3J = 8.3 Hz, ^3J = 7.3 Hz, 2H, Ar$H_{3/6}$),), 7.37 – 7.28 (m, 5H, NCH$_2$*Ph*), 7.06 (d, ^3J = 2.0 Hz, 1H$_{imidazolylidene}$), 6.68 (d, ^3J = 2.0 Hz, 1H$_{imidazolylidene}$), 5.85 (d, ^3J = 14.9 Hz, 2H, NCH_2Ph), 5.71 (d, ^3J = 14.8 Hz, 2H, NCH_2Ph), 4.96 (td, ^4J = 4.6 Hz, 1H, C*H*-COD), 4.84 (td, ^4J = 6.4 Hz, 2H, C*H*-COD), 4.73 (dt, ^3J = 8.3, 2H, NCH_2CH$_3$-), 4.39 (dt, ^3J = 7.3 Hz, 2H, -CH$_2$CH_2N), 3.37 – 3.24 (m, 2H, C*H*-COD), 2.60 – 2.10 (m, 8H, CH_2-COD), 1.95 – 1.75 (m, 2H, NCH$_2$CH_2-); ^{13}C NMR ($CDCl_3$): (ppm) δ 183.37

(NHC), 164.25 (CO), 136.54 (ArC), 134.07 (ArC), 131.59 (ArC), 131.36 (ArC), 128.84 (ArC), 128.26 (ArC), 128.19 (ArC), 128.03 (ArC), 126.98 (ArC), 122.59 (ArC), 120.63 ($CH_{imidazolylidene}$), 98.57 (dd, ^4J = 7.0 Hz, ^4J = 2.7 Hz, 2C, CH-COD), 68.20 (d, J = 3.4 Hz, 2C, C*H*-COD), 68.06 (d, J = 3.1 Hz, 2C, C*H*-COD), 54.60 (N<u>C</u>H_2Ph), 48.67 (NCH_2-), 37.98 (NCH_2-), 33.01 (CH_2-COD), 32.72 (CH_2-COD), 29.46 (NCH_2<u>C</u>H_2CH_2N), 28.85 (CH_2-COD), 28.64 (CH_2-COD); MS(ESI): 606.16 (M + Cl^-); elemental analysis for $C_{33}H_{33}N_3O_2ClRh$ (% calcd/found): C (61.74/61.30), H (5.18/5.23), N (6.55/6.38).

Dichloro[1-(3'-(1'',8''-naphthalimid-N''-yl))-propyl-3-methyl-imidazol-2-ylidene] (η^6-p-cymene)ruthenium(II) (**5a**).

Yield: 0.073 g (0.12 mmol, 47%) red/brown solid; melting point: 214–215 °C; ^{1}H NMR ($CDCl_3$): (ppm) δ 8.61 (dd, ^3J = 7.3 Hz, ^4J = 1.2 Hz, 2H, Ar$H_{4/5}$), 8.22 (dd, ^3J = 8.4 Hz, ^4J = 1.2 Hz, 2H, Ar$H_{2/7}$), 7.76 (dd, ^3J = 8.3 Hz, ^3J = 7.3 Hz, 2H, Ar$H_{3/6}$), 7.11 (d, ^3J = 2.0 Hz, 1H$_{imidazolylidene}$), 6.96 (d, ^3J = 2.0 Hz, 1H$_{imidazolylidene}$), 5.34-4.92 (m, ^3J = 6.1 Hz, 4H, MeC_6H_4-), 4.82 (t, ^3J = 12.2 Hz, 1H, -CH_2CH_2N), 4.33 (t, ^3J = 6.2 Hz, 2H, NCH_2CH_2-), 4.11 (t, ^3J = 12.2 Hz, 1H, -CH_2CH_2N), 3.95 (s, 3H, NCH_3), 2.59 (hept, ^3J = 6.9 Hz, 1H, C*H*(Me)$_2$), 2.32 (dd, ^3J = 8.0 Hz, 2H, NCH_2CH_2-), 1.86 (s, 3H, -$C_6H_4CH_3$), 1.08 (d, ^3J = 6.9 Hz, 6H, ((CH_3)$_2$$CHC_6H_4$–); ^{13}C NMR ($CDCl_3$): (ppm) δ 174.39 (NHC), 164.66 (CO), 133.83 (ArC), 131.67 (ArC), 130.99 (ArC), 128.46 (ArC), 126.83 (ArC), 123.98 (ArC), 123.14 ($CH_{imidazolylidene}$), 121.16 ($CH_{imidazolylidene}$), 108.52 and 99.94 (quaternary C from *p*-cymene), 84.62 and 85.44 (CH from *p*-cymene), 49.77 (NCH_2-), 39.47 (NCH_3), 37.68 (NCH_2-), 30.54 (–<u>C</u>H(CH_3)$_2$), 30.27 (NCH_2<u>C</u>H_2CH_2N), 18.43 (-CH(<u>C</u>H_3)$_2$); MS(ESI): 590.11 (M+ + Cl^-); elemental analysis for $C_{29}H_{31}N_3O_2Cl_2Ru$ (% calcd/found): C (55.68/55.26), H (5.00/5.00), N (6.72/6.67).

Dichloro[1-(3'-(1'',8''-naphthalimid-N''-yl))-propyl-3-ethyl-imidazol-2-ylidene](η^6-p-cymene)ruthenium(II) (**5b**)

Yield: 0.092 g (0.15 mmol, 58%) red/brown crystals; melting point: 206–208 °C; ^{1}H NMR ($CDCl_3$): (ppm) δ 8.61 (dd, ^3J = 7.2 Hz, ^4J = 1.1 Hz, 2H, Ar$H_{4/5}$), 8.23 (dd, ^3J = 8.3 Hz, ^4J = 1.1 Hz, 2H, Ar$H_{2/7}$), 7.76 (dd, ^3J = 8.2 Hz, ^3J = 7.2 Hz, 2H, Ar$H_{3/6}$), 7.13 (d, ^3J = 2.1 Hz, 1H$_{imidazolylidene}$), 7.04 (d, ^3J = 2.1 Hz, 1H$_{imidazolylidene}$), 5.28 (d, ^3J = 5.8 Hz, 1H, MeC_6H_4-), 5.11 (dd, , ^3J = 24.1 Hz, 2H, MeC_6H_4-), 4.93 (d, ^3J = 5.7 Hz, 1H, MeC_6H_4-), 4.73 (dq, ^3J = 7.2 Hz, 2H, NCH_2CH_3), 4.34 (dt, ^3J = 6.1, ^4J = 1.7 Hz, 2H, NCH_2CH_2-), 4.03 (dt, ^3J = 10.0 Hz, 2H, -CH_2CH_2N) 2.59 (hept, ^3J = 6.9 Hz, 1H, -C*H*(CH_3)$_2$), 2.52-2.36 (p, 1H, NCH_2CH_2-), 2.28-2.12 (p, 1H, NCH_2CH_2-), 1.84 (s, 3H, -$C_6H_4CH_3$), 1.40 (t, ^3J = 7.2 Hz, 3H, NCH_2CH_3), 1.07 (d, ^3J = 6.9 Hz, 6H, (CH_3)$_2$$CHC_6H_4$-); (600 MHz, DMSO-$d_6$): (ppm) δ 8.59 – 8.46 (m, 4H, Ar$H_{4/5}$, Ar$H_{2/7}$), 7.91 (q, ^3J = 7.9 Hz, 2H, Ar$H_{3/6}$), 7.85 (d, ^3J = 2.1 Hz, 1H$_{imidazolylidene}$), 7.79 (d, ^3J = 2.1 Hz, 1H$_{imidazolylidene}$), 7.58 (d, ^3J = 2.1 Hz, 1H$_{imidazolylidene}$), 7.52 (d, ^3J = 2.1 Hz, 1H$_{imidazolylidene}$),

6.08 (d, ^3J = 6.3 Hz,1H, MeC$_6H_4$-), 5.98 (d, , ^3J = 6.2 Hz, 1H, MeC$_6H_4$-), 5.69 (d, ^3J = 6.3 Hz, 1H, MeC$_6H_4$-), 4.96 (d, ^3J = 5.8 Hz, 1H, MeC$_6H_4$-), 4.52 (m, ^3J = 5.0 Hz, 1H, -CH_2CH$_2$N), 4.31 – 4.01 (m, 4H, NCH_2CH$_2$CH_2N), 3.95 (m, ^3J = 4.8 Hz, 1H, -CH_2CH$_2$N), 2.71 (m, 1H, 1H, -CH(CH$_3$)$_2$), 2.33 (q, 2H, NCH_2CH$_3$), 2.24 (q, 2H, NCH_2CH$_3$), 1.86 (s, 3H, -C$_6$H$_4$CH_3), 1.68 (s, 3H, -C$_6$H$_4$CH_3), 1.41 (t, ^3J = 7.2 Hz, 3H, NCH$_2$CH_3), 1.29 (t, J = 7.1 Hz, 3H, NCH$_2$CH_3), 1.16 (d, J = 6.9 Hz, 3H, (CH_3)$_2$CHC$_6$H$_4$-), 1.12 (d, J = 6.8 Hz, 3H, (CH_3)$_2$CHC$_6$H$_4$-) 1.03 (d, J = 6.9 Hz, 3H, (CH_3)$_2$CHC$_6$H$_4$-), 0.85 (d, J = 6.8 Hz, 3H, (CH_3)$_2$CHC$_6$H$_4$-); ^{13}C NMR (CDCl$_3$): (ppm) δ 174.06 (NHC), 164.47 (CO), 133.60 (ArC), 131.45 (ArC), 130.86 (ArC), 130.74 (ArC), 128.27 (ArC), 126.77 (ArC), 121.22 (CH$_{imidazolylidene}$), 121.20 (CH$_{imidazolylidene}$), 107.89 and 100.06 (quaternary C from *p*-cymene), 84.32, 84.10, 83.66, 81.61 (CH from *p*-cymene), 49.50 (NCH$_2$-), 45.99 (N<u>C</u>H$_2$CH$_3$), 37.43 (NCH$_2$-), 30.25 (–CH(C**H**$_3$)$_2$), 30.02 (NCH$_2$<u>C</u>H$_2$CH$_2$N), 21.53 (C$_6$H$_4$<u>C</u>H$_3$), 18.20 (CH(<u>C</u>H$_3$)$_2$), 16.56 (NCH$_2$CH$_3$); MS(ESI): 604.13 (M + Cl$^-$); elemental analysis for C$_{30}$H$_{34}$N$_3$O$_2$Cl$_2$Ru (% calcd/found): C (56.34/56.34), H (5.20/5.15), N (6.57/6.43).

Dichloro[1-(3'-(1'',8''-naphthalimid-N''-yl))-propyl-3-benzyl-imidazol-2-ylidene] (η^6-p-cymene)ruthenium(II) (**5c**)

Yield: 0.101 g (0.15 mmol, 58%) red/brown solid; melting point: 153–155 °C; ^{1}H NMR (CDCl$_3$): (ppm) δ 8.62 (dd, ^3J = 7.2 Hz, ^4J = 1.1 Hz, 2H, Ar$H_{4/5}$), 8.23 (dd, ^3J = 8.3 Hz, ^4J = 1.1 Hz, 2H, Ar$H_{2/7}$), 7.77 (dd, ^3J = 8.3 Hz, ^3J = 7.3 Hz, 2H, Ar$H_{3/6}$), 7.37 – 7.25 (m, 5H, NCH$_2$*Ph*), 7.11 (d, ^3J = 2.1 Hz, 1H$_{imidazolylidene}$), 6.83 (d, ^3J = 2.0 Hz, 1H$_{imidazolylidene}$), 5.77 (d, ^3J = 14.1 Hz, 1H, NCH_2Ph), 5.56 (d, ^3J = 14.8 Hz, 1H, NCH_2Ph), 5.17 (d, ^3J = 5.6 Hz, 2H, MeC$_6H_4$), 5.04 (d, ^3J = 5.7 Hz, 1H, MeC$_6H_4$), 4.95 (t, ^3J = 13.3 Hz, 1H, -CH$_2$CH_2N), 4.80 (d, ^3J = 4.2, 1H, MeC$_6H_4$), 4.36 (t, ^3J = 6.2 Hz, 2H, NCH_2CH$_3$-), 4.11 (t, ^3J = 13.3 Hz, 1H, -CH$_2$CH_2N), 2.74 (p, ^3J = 7.0 Hz, 1H, -CH(Me)$_2$), 2.32 (m, 2H, -CH_2CH$_2$N), 1.94 (s, 3H, -C$_6$H$_4$CH_3), 1.12 (d, ^3J = 6.9 Hz, 6H, (CH_3)$_2$CHC$_6$H$_4$-); ^{13}C NMR (CDCl$_3$): (ppm) δ 175.51 (NHC), 164.65 (CO), 137.44 (ArC), 133.85 (ArC), 131.69 (ArC), 130.97 (ArC), 128.71 (ArC), 128.49 (ArC), 127.96 (ArC), 127.87 (ArC), 126.84 (ArC), 123.15 (ArC), 121.24 (CH$_{imidazolylidene}$), 108.15 and 99.66 (quaternary C from *p*-cymene), 85.58 and 82.37 (CH from *p*-cymene), 54.74 (-CH$_2$Ph), 49.99 (NCH$_2$-), 37.72 (NCH$_2$-), 30.49 (–<u>C</u>H(C**H**$_3$)$_2$), 30.28 (NCH$_2$<u>C</u>H$_2$CH$_2$N), 26.90 (C$_6$H$_4$<u>C</u>H$_3$), 18.60 (CH(<u>C</u>H$_3$)$_2$); MS(ESI): 666.15 (M + Cl$^-$); elemental analysis for C$_{35}$H$_{35}$N$_3$O$_2$Cl$_2$Ru (% calcd/found): C (59.91/59.57), H (5.03/4.92), N (5.99/5.58).

Bromido[1-(3'-(1'',8''-naphthalimid-N''-yl))-propyl-3-methyl-imidazol-2-ylidene]copper(I) (**6a**)

Yield: 0.046 g (0.10 mmol, 40%) white solid; melting point: 149–151 °C (thermal decomposition); ^{1}H NMR (CDCl$_3$): (ppm) δ 8.54 (dd, ^3J = 7.3 Hz, ^4J = 1.6 Hz, 2H, Ar$H_{4/5}$), 8.17 (dd, ^3J = 9.2 Hz, ^4J = 1.2 Hz, 2H, Ar$H_{2/7}$), 7.71 (dd, ^3J = 7.8 Hz, ^3J = 7.0 Hz, 2H, Ar$H_{3/6}$),), 6.31 (d, ^3J = 3.0 Hz, 1H$_{imidazolylidene}$), 6.11 (d, ^3J = 3.0 Hz, 1H$_{imidazolylidene}$), 3.69 (t, ^3J = 7.2

Hz, 2H, NCH_2CH$_3$-), 3.17 (s, 3H, NCH_3), 2.26 (t, ^3J = 6.7 Hz, 2H, -CH$_2$CH_2N), 2.07 (p, ^3J = 14.3 Hz, 2H, -CH_2CH$_2$N); ^{13}C NMR ($CDCl_3$): (ppm): δ 164.23 (NHC), 153.27 (CO) 134.24 (ArC), 134.03 (ArC), 131.51 (ArC), 131.30 (ArC), 127.01 (ArC), 126.95 (ArC), 111.33 ($CH_{imidazolylidene}$), 109.92 ($CH_{imidazolylidene}$), 41.44 (NCH_2-), 37.87 (NCH_2-), 37.45 (NCH_3) 29.82 ($NCH_2\underline{C}H_2CH_2N$); MS(ESI): 320.14 (M + CuBr); elemental analysis for $C_{19}H_{17}N_3O_2CuBr$ (% calcd/found): C (49.31/48.61), H (3.70/4.09), N (9.08/8.74).

Bromido[1-(3'-(1'',8''-naphthalimid-N''-yl))-propyl-3-ethyl-imidazol-2-ylidene]copper(I) (**6b**)
Yield: 0.046 g (0.10 mmol, 40%) white solid; melting point: 150–153 °C (thermal decomposition); ^{1}H NMR ($CDCl_3$): (ppm) δ 8.61 (dd, ^3J = 7.1 Hz, ^4J = 1.2 Hz, 2H, Ar$H_{4/5}$), 8.25 (dd, ^3J = 8.3 Hz, ^4J = 1.1 Hz, 2H, Ar$H_{2/7}$), 7.78 (dd, ^3J = 8.2 Hz, ^3J = 7.7 Hz, 2H, Ar$H_{3/6}$),), 7.16 (d, ^3J = 1.1 Hz, 1H$_{imidazolylidene}$), 6.94 (d, ^3J = 1.1 Hz, 1H$_{imidazolylidene}$), 4.68 (q, ^3J = 8.6 Hz, 2H, NCH_2CH$_3$), 4.26 (dt, ^3J = 14.2 Hz, 2H, NCH_2CH$_2$-), 4.37 (dt, ^3J = 7.5 Hz, 2H, -CH$_2$CH_2N), 2.34 (m, ^3J = 7.0 Hz 2H, -CH_2CH$_2$N), 1.51 (t, ^3J = 7.3 Hz, 3H, NCH$_2$CH_3); ^{13}C NMR ($CDCl_3$): (ppm): δ 164.02 (CO), 134.02 (NHC), 133.81 (ArC), 131.39 (ArC), 131.29 (ArC), 127.97 (ArC), 126.79 (ArC), 122.15 (ArC), 120.41 ($CH_{imidazolylidene}$), 119.66 ($CH_{imidazolylidene}$), 49.13 (NCH_2-), 46.30 (-$\underline{C}H_2CH_3$), 37.27 (NCH_2-), 29.60 ($NCH_2\underline{C}H_2CH_2N$), 16.72 (-CH$_2\underline{C}H_3$); MS(ESI): 396.07 (M + Br$^-$); elemental analysis for $C_{20}H_{19}N_3O_2CuBr$ (% calcd/found): C (50.38/50.04), H (4.02/3.85), N (8.81/8.34).

Bromido[1-(3'-(1'',8''-naphthalimid-N''-yl))-propyl-3-benzyl-imidazol-2-ylidene]copper(I) (**6c**)
Yield: 0.117 g (0.28 mmol, 87%) white solid; melting point: 190–193 °C (thermal decomposition); ^{1}H NMR ($CDCl_3$): (ppm) δ 8.61 (dd, ^3J = 7.3 Hz, ^4J = 1.2 Hz, 2H, Ar$H_{4/5}$), 8.24 (dd, ^3J = 8.3 Hz, ^4J = 1.1 Hz, 2H, Ar$H_{2/7}$), 7.78 (dd, ^3J = 8.3 Hz, ^3J = 7.3 Hz, 2H, Ar$H_{3/6}$), 7.40-7.27 (m, 5H, NCH$_2$*Ph*), 7.16 (d, ^3J = 1.8 Hz, 1H$_{imidazolylidene}$), 6.87 (d, ^3J = 2.4 Hz, 1H$_{imidazolylidene}$), 6.38 (d, ^3J = 3.0 Hz, 1H, CH_2Ph), 6.13 (d, ^3J = 3.0 Hz, 1H, CH_2Ph), 4.28 (dt, ^3J = 14.4 Hz, 4H, NCH_2CH$_2$CH_2N), 2.35 (p, ^4J = 6.9 Hz, 2H, -CH_2CH$_2$N); ^{13}C NMR ($CDCl_3$): (ppm): δ 164.24 (CO), 135.52 (NHC), 134.24 (ArC), 131.59 (ArC), 131.52 (ArC), 131.36 (ArC), 129.11 (ArC), 128.62 (ArC), 128.19 (ArC), 127.96 (ArC), 127.02 (ArC), 126.98 (ArC), 122.59 ($CH_{imidazolylidene}$), 122.40 ($CH_{imidazolylidene}$), 55.43 (-CH$_2$PH), 49.44 (NCH_2-), 37.49 (NCH_2-), 29.97 ($NCH_2\underline{C}H_2CH_2N$); MS(ESI): 396.17 (M + CuBr); elemental analysis for $C_{25}H_{21}N_3O_2CuBr$ (% calcd/found): C (55.72/55.76), H (3.93/4.04), N (7.80/7.32).

X-ray crystallography

Single crystals were obtained from dichloromethane / diethyl ether (1:3). Crystal data are summarized in Table S1 (see Supporting Information). The crystal was mounted in inert oil on a glass fibre and transferred to the cold gas stream of an Oxford Diffraction Nova A

diffractometer. Intensity measurements were performed using mirror-focussed Cu *Kα* radiation (λ = 1.54184 Å). Absorption corrections were based on multi-scans. Structures were refined anisotropically on F^2 using the program SHELXL-97[22]. Hydrogen atoms were included using a riding model or rigid methyl groups. Compound **5b** crystallized only by chance in the chiral (Sohncke) space group $P2_1$; the Flack parameter refined to –0.021(6). CCDC 1510249 contains the complete supplementary crystallographic data for this paper. These data can be obtained free of charge from the Cambridge Crystallographic Data Centre via http://www.ccdc.cam.ac.uk/.

Antiproliferative effects in MCF-7 and HT-29 cells

MCF-7 breast adenocarcinoma and HT-29 colon carcinoma cells were maintained in DMEM High Glucose (PAA) supplemented with 50 mg/L gentamycin and 10% (v/v) fetal bovine serum (FBS) prior to use. The antiproliferative effects of the compounds were determined following an established procedure. In short, cells were suspended in cell culture medium (HT-29: 3000 cells mL^{-1}, MCF-7: 10 000 cells mL^{-1}), and 100 µL aliquots thereof were plated in 96-well plates and incubated at 37 °C: 5 % CO_2 for 48 h (HT-29) or 72 h (MCF-7). Stock solutions of the ruthenium complexes in DMF were freshly prepared and diluted with cell culture medium to the desired concentrations (final DMF concentration: 0.1 % v/v). The medium in the plates was replaced with medium containing the compounds in graded concentrations (six replicates, 200 µL per well). After further incubation for 72 h (HT-29) or 96 h (MCF-7) the cell biomass was determined by crystal violet staining and the IC_{50} values were determined as those concentrations causing 50 % inhibition of cell proliferation. Results are represented as means of independent experiments.

Solution Stability

Solution stability of rhodium- (**4b**) and ruthenium- (**5b**) complexes was measured via ^{1}H NMR and ESI mass spectroscopies. For this purpose, the compounds were dissolved in dimethyl sulfoxide (DMSO) at 10 mM concentration. The NMR results were obtained from the same probe measured after various periods. For ESI MS experiments aliquots of the substance dissolved in DMSO were withdrawn at different time points and investigated. ^{1}H NMR spectra were recorded on a Bruker AV II-600 AS NMR spectrometer. Chemical shifts are reported in parts per million and referenced to the residual solvent peak: DMSO: ^{1}H δ 2.50. Electrospray ionization ion-trap mass spectrometry (ESI-IT MS) was used for additional stability studies on complex **5b**.

DNA-binding study with UV-vis spectroscopy

UV-vis absorption measurements were recorded at 25 °C on a PerkinElmer LAMBDA 35 double beam spectrophotometer, equipped with a Peltier temperature controller, using 1 cm path-length cuvettes. The titrations were carried out by adding increasing amounts of DNA (ct-DNA) stock solution to a metal-complex solution with constant concentration. To ensure that during the titration the concentration of the selected metal complex remained unaltered, for each addition of the DNA solution, the same volume of a doubly-concentrated metal complex solution was added. For Kb calculation, the binding model was used as a script for the nonlinear curve fitting operation of Origin (OriginLab, Northampton, MA), as reported by Hargrove et al [23].

DNA interaction by CD spectroscopy

Circular dichroism spectra were recorded at 25 °C on a Chirascan™ CD Spectrometer (by AppliedPhotophisics) using 1 cm path-length quartz cells. Throughout the experiment, the concentration of the DNA was kept constant while increasing amounts of a metal-complex were added.

DNA binding: Reaction with 9-Ethylguanine

1.0 mM stock solutions of compounds **4b** and **5b** were prepared in methanol. Aliquots of these were mixed with MilliQ water solutions of 9-EtG and stirred for 2 h at room temperature. Final concentrations were 0.2 mM for the metal compounds and 0.6 mM for 9-EtG. The resulting mixtures were analysed by MS. Mass spectrometry was performed in the positive-ion mode on a maXis classic (Bruker Daltonik GmbH, Bremen, Germany) hybrid ESI-Qq/oa-TOF MS instrument. Samples were diluted in acetonitrile/MeOH 1% H_2O and the introduction was performed via direct infusion. The following parameters were used: flow rate 3 µL/min; capillary voltage -4500 V; dry gas flow 4.0 L/min (nitrogen); dry temperature 180 °C; resolution: 20000 FWHM; mass accuracy < 5ppm.

Apoptosis effects on MelHO, MelHO bcl-2, Nalm-6 and BJAB cells

MelHO (human melanoma cells) pIres and MelHO bcl-2 (transfected MelHO cells with the vector pIres and the bcl-2 gene, thus overexpressing the anti-apoptotic protein Bcl-2) were kindly provided by Peter Daniel, Charité, Berlin, Germany; Nalm-6 (human B cell precursor leukemia cells) were kindly provided by Dr. Seeger, Charité, Berlin; vincristine-, daunorubicine-, and prednisolone-resistant Nalm-6 cells (NaKu) and also vincristine- and doxorubicin-resistant BJAB cells were generated by Dr. Prokop, Children‘s Hospital Cologne, Germany. In order to generate drug resistant cell lines, Nalm-6 cells were exposed to increasing concentrations of selected drugs as soon as they tolerated high concentrations without loss of vitality. By this method, a vincristine-resistant Nalm-6 cell line (Nalm-6/VCR)

and a daunorubicine-resistant Nalm-6 cell line (Nalm-6/DNR) were produced. The cells were subcultured every 3-4 days by dilution of the cells to a concentration of $1x10^5$/ml. All experiments were performed in RPMI 1640 (GIBCO, Invitrogen) supplemented with 10% heat-inactivated fetal calf serum, 100 U/ml penicillin, 100 µg/ml streptomycin, and 0.56 g/l L-glutamine. The assay was set up 24 h in advance, and cells were cultured at a concentration of $3x10^5$/ml to attain standardized growth conditions. For apoptosis assays, the cells were then diluted to a concentration of $1x10^5$/ml immediately before the addition of various drugs.

Measurement of DNA fragmentation

Apoptotic cell death was determined by a modified cell cycle analysis, which detects DNA fragmentation at the single cell level. Cells were seeded at a density of $1x10^5$ cells/ml and treated with various concentrations of **4b**. After a 72-h incubation period at a temperature of 37°C, cells were collected by centrifugation at 1500 rpm for 5 min, washed with PBS at 4°C, and fixed in PBS/2% (v/v) formaldehyde on ice for 30 min. After fixation, cells were pelleted, incubated with ethanol/PBS (2:1, v/v) for 15 min, pelleted and resuspended in PBS containing 40 µg/ml RNase. RNA was digested for 30 min at a temperature of 37°C, after which the cells were pelleted again and finally resuspended in PBS containing 50 µg/ml propidium iodide. Nuclear DNA fragmentation was quantified by flow cytometric determination of hypodiploid DNA. Data were collected and analyzed using a flow cytometry analysis by FACScan (Becton–Dickinson, Heidelberg, Germany) equipped with CELL Quest software. Data are given in percent hypoploidy (subG1), which reflects the number of apoptotic cells.

Measurement of the mitochondrial permeability transition (Δψm)

After an incubation period of 48 h with various concentrations of **4b**, the cells were collected by centrifugation at 1500 rpm, 4°C for 5 min. The mitochondrial permeability transition was then determined by staining the cells with 5,50,6,60-tetrachloro-1,10,3,30-tetraethyl-benzimidazolylcarbocyanine iodide (JC-1; Molecular Probes, Leiden, The Netherlands). Then $1x10^5$ cells were resuspended in 500 µL phenol red-free RPMI 1640 without supplements, and JC-1 was added to give a final concentration of 2.5 µg ml^{-1}. The cells were incubated for 30 min at 37°C with moderate shaking. Control cells were likewise incubated in the absence of JC-1 dye. The cells were harvested by centrifugation at 1500 rpm, 4°C for 5 min, washed with ice-cold PBS, and resuspended in 200 µl PBS at 4°C. Mitochondrial permeability transition was then quantified by flow cytometric determination of the cells with decreased fluorescence, i.e. with mitochondria displaying a lower membrane potential. Data were collected and analyzed using a FACScan (Becton-Dickinson, Heidelberg, Germany)

apparatus equipped with the CELL Quest software. Data are given in % cells with low Δψm, which reflects the number of cells undergoing mitochondrial apoptosis.

References

[1] a) L. Oehninger, R. Rubbiani, I. Ott, *Dalton Trans* **2013**, *42*(10), 3269-3284; b) F. Cisnetti, A. Gautier, *Angewandte Chemie* **2013**; c) W. Liu, R. Gust, *Coord. Chem. Rev.* **2016**, *329*, 191-213.
[2] a) B. Bertrand, L. Stefan, M. Pirrotta, D. Monchaud, E. Bodio, P. Richard, P. Le Gendre, E. Warmerdam, M. H. de Jager, G. M. Groothuis, M. Picquet, A. Casini, *Inorg. Chem.* **2014**, *53*(4), 2296-2303; b) J.-J. Zhang, C.-M. Che, I. Ott, *J. Organomet. Chem.* **2015**, *782*, 37-41; c) J. J. Zhang, J. K. Muenzner, M. A. Abu El Maaty, B. Karge, R. Schobert, S. Wölfl, I. Ott, *Dalton Trans.* **2016**, *45*(33), 13161-13168; d) A. Kascatan-Nebioglu, A. Melaiye, K. Hindi, S. Durmus, M. J. Panzner, L. A. Hogue, R. J. Mallett, C. E. Hovis, M. Coughenour, S. D. Crosby, A. Milsted, D. L. Ely, C. A. Tessier, C. L. Cannon, W. J. Youngs, *J. Med. Chem.* **2006**, *49*, 6811-6818.
[3] S. D. Köster, H. Alborzinia, S. Can, I. Kitanovic, S. Wölfl, R. Rubbiani, I. Ott, P. Riesterer, A. Prokop, K. Merz, N. Metzler-Nolte, *Chem. Sci.* **2012**, *3*, 2062-2072.
[4] J. K. Muenzner, B. Biersack, H. Kalie, I. C. Andronache, L. Kaps, D. Schuppan, F. Sasse, R. Schobert, *ChemMedChem* **2014**, *9*(6), 1195-1204.
[5] A. Meyer, L. Oehninger, Y. Geldmacher, H. Alborzinia, S. Wolfl, W. S. Sheldrick, I. Ott, *ChemMedChem* **2014**, *9*(8), 1794-1800.
[6] a) M. F. Brana, A. Ramos, *Curr. Med. Chem. - Anti-Cancer Agents* **2001**, *1*, 237-255; b) M. F. Brana, M. Cacho, M. A. Garcia, B. d. Pascual-Teresa, A. Ramos, M. T. Dominguez, J. M. Pozuelo, C. Abradelo, M. F. Rey-Stolle, M. Yuste, M. Banez-Coronel, J. C. Lacal, *J. Med. Chem.* **2004**, *47*, 1391-1399; c) S. Banerjee, E. B. Veale, C. M. Phelan, S. A. Murphy, G. M. Tocci, L. J. Gillespie, D. O. Frimannsson, J. M. Kelly, T. Gunnlaugsson, *Chem. Soc. Rev.* **2013**, *42*(4), 1601-1618; d) Z. Chen, X. Liang, H. Zhang, H. Xie, J. Liu, Y. Xu, W. Zhu, Y. Wang, X. Wang, S. Tan, D. Kuang, X. Qian, *J. Med. Chem.* **2010**, *53*, 2589-2600.
[7] a) J. M. Perez, I. Lopez-Solera, E. I. Montero, M. F. Brana, C. Alonso, S. P. Robinson, C. Navarro-Ranninger, *J. Med. Chem.* **1999**, *42*(26), 5482-5486; b) S. Banerjee, J. A. Kitchen, S. A. Bright, J. E. O'Brien, D. C. Williams, J. M. Kelly, T. Gunnlaugsson, *Chem. Commun.* **2013**, *49*(76), 8522-8524; c) C. P. Bagowski, Y. You, H. Scheffler, D. H. Vlecken, D. J. Schmitz, I. Ott, *Dalton Trans.* **2009**, 10799-10805; d) I. Ott, X. Qian, Y. Xu, D. H. Vlecken, I. J. Marques, D. Kubutat, J. Will, W. S. Sheldrick, P. Jesse, A. Prokop, C. P. Bagowski, *J. Med. Chem.* **2009**, *52*(3), 763-770; e) G. J. Ryan, F. E. Poynton, R. B. Elmes, M. Erby, D. C. Williams, S. J. Quinn, T. Gunnlaugsson, *Dalton Trans.* **2015**, *44*(37), 16332-16344; f) S. Tan, K. Han, Q. Li, L. Tong, Y. Yang, Z. Chen, H. Xie, J. Ding, X. Qian, Y. Xu, *Eur. J. Med. Chem.* **2014**, *85*, 207-214.
[8] a) L. Oehninger, M. Stefanopoulou, H. Alborzinia, J. Schur, S. Ludewig, K. Namikawa, A. Muñoz-Castro, R. W. Köster, K. Baumann, S. Wölfl, W. S. Sheldrick, I. Ott, *Dalton Trans.* **2013**, *42*, 1657–1666; b) L. Oehninger, H. Alborzinia, S. Ludewig, K. Baumann, S. Wölfl, I. Ott, *ChemMedChem* **2011**, *6*(12), 2142-2145.
[9] a) J. R. McConnell, D. P. Rananaware, D. M. Ramsey, K. N. Buys, M. L. Cole, S. R. McAlpine, *Bioorg. Med. Chem. Lett.* **2013**, *23*, 2527-2531; b) L. Oehninger, S. Spreckelmeyer, P. Holenya, S. M. Meier, S. Can, H. Alborzinia, J. Schur, B. K. Keppler, S. Wölfl, I. Ott, *J. Med. Chem.* **2015**, *58*(24), 9591-9600; c) L. Oehninger, L. N. Kuster, C. Schmidt, A. Munoz-Castro, A. Prokop, I. Ott, *Chem. Eur. J.* **2013**, *19*(52), 17871-17880.
[10] a) M. Teyssot, A. Jarrousse, A. Chevry, A. D. Haze, C. Beaudoin, M. Manin, S. P. Nolan, S. Diez-Gonzalez, L. Morel, A. Gautier, *Chem. Eur. J.* **2009**, *15*, 314-318; b) W. Streciwilk, F. Hackenberg, H. Müller-Bunz, M. Tacke, *Polyhedron* **2014**, *80*, 3-9; c) W. Walther, I. Fichtner, F. Hackenberg, W. Streciwilk, M. Tacke, *Letters Drug. Des. Drug. Disc.* **2014**, *11*, 825-832.
[11] a) R. M. Duke, E. B. Veale, F. M. Pfeffer, P. E. Kruger, T. Gunnlaugsson, *Chem. Soc. Rev.* **2010**, *39*, 3936-3953; b) E. E. Langdon-Jones, N. O. Symonds, S. E. Yates, A. J. Hayes, D. Lloyd, R. Williams, S. J. Coles, P. N. Horton, S. J. Pope, *Inorg. Chem.* **2014**,

53(7), 3788-3797; c) X. Poteau, A. I. Brown, R. G. Brown, C. Holmes, D. Matthew, *Dyes Pigm.* **2000**, *47*, 91-105.
[12] a) C. R. Groom, F. H. Allen, *Angew. Chem. Int. Ed. Engl.* **2014**, *53*(3), 662-671; b) C. R. Groom, I. J. Bruno, M. P. Lightfoot, S. C. Ward, *Acta Crystallogr. B Struct. Sci. Cryst. Eng. Mater.* **2016**, *72*(Pt 2), 171-179.
[13] I. Bratsos, S. Calmo, E. Zangrando, G. Balducci, E. Alessio, *Inorg. Chem.* **2013**, *52*(20), 12120-12130.
[14] S. Banerjee, J. A. Kitchen, T. Gunnlaugsson, J. M. Kelly, *Org. Biomol. Chem.* **2012**, *10*(15), 3033-3043.
[15] F. M. Pohl, T. M. Jovin, W. Baehr, J. J. Holbrook, *Proc. Natl. Acad. Sci. U S A* **1972**, *69*(12), 3805-3809.
[16] P. Thordarson, *Chem. Soc. Rev.* **2011**, *40*(3), 1305-1323.
[17] K. J. Kilpin, C. M. Clavel, F. Edafe, P. J. Dyson, *Organometallics* **2012**, *31*, 7031−7039.
[18] a) S. Betanzos-Lara, L. Salassa, A. Habtemariam, P. J. Sadler, *Chem. Commun.* **2009**(43), 6622-6624; b) J. Ruiz, V. Rodriguez, N. Cutillas, A. Espinosa, M. J. Hannon, *Inorg. Chem.* **2011**, *50*(18), 9164-9171; c) W. Zheng, Q. Luo, Y. Lin, Y. Zhao, X. Wang, Z. Du, X. Hao, Y. Yu, S. Lu, L. Ji, X. Li, L. Yang, F. Wang, *Chem. Commun.* **2013**, *49*(87), 10224-10226; d) H. Chen, J. A. Parkinson, R. E. Morris, P. J. Sadler, *J. Am. Chem. Soc.* **2003**, *125*(1), 173-186.
[19] R. Rubbiani, I. Kitanovic, H. Alborzinia, S. Can, A. Kitanovic, L. A. Onambele, M. Stefanopoulou, Y. Geldmacher, W. S. Sheldrick, G. Wolber, A. Prokop, S. Wölfl, I. Ott, *J. Med. Chem.* **2010**, *53*, 8608–8618.
[20] a) R. E. Morris, R. E. Aird, P. d. S. Murdoch, H. Chen, J. Cummings, N. D. Hughes, S. Parsons, A. Parkin, G. Boyd, D. I. Jodrell, P. J. Sadler, *J. Med. Chem.* **2001**, *44*, 3616-3621; b) C. Scolaro, C. G. Hartinger, C. S. Allardyce, B. K. Keppler, P. J. Dyson, *J. Inorg. Biochem.* **2008**, *102*, 1743–1748.
[21] a) A. Levina, A. Mitra, P. A. Lay, *Metallomics* **2009**, *1*, 458-470; b) M. I. Webb, R. A. Chard, Y. M. Al-Jobory, M. R. Jones, E. W. Wong, C. J. Walsby, *Inorg. Chem.* **2012**, *51*(2), 954-966.
[22] G. M. Sheldrick, *Acta Crystallogr. A* **2008**, *64*(Pt 1), 112-122.
[23] A. E. Hargrove, Z. Zhong, J. L. Sessler, E. V. Anslyn, *New J. Chem.* **2010**, *34*(2), 348-354.